ADVANCED FUNCTIONAL MATERIALS
www.afm-journal.de

Check for updates

Recent Advances in Twisted Structures of Flatland Materials and Crafting Moiré Superlattices

Ghulam Abbas, Yu Li, Huide Wang, Wen-Xing Zhang, Cong Wang, and Han Zhang**

The past decade has witnessed the occurrence of novel 2D moiré patterns in nanoflatland materials. These visually beautiful moiré superlattices have become a playground on which exotic quantum phenomena can be observed. The state-of-the-art experimental techniques that have been developed for crafting moiré superlattices of flatland materials are reviewed. Graphene and its heterostructure with boron nitride have now sparked new interlayer twists as a new degree of freedom for tuning several angle-dependent physical properties, e.g., the appearance of van Hove singularities, tunable Mott insulator states, and the Hofstadter butterfly pattern. Moreover, the interplay of correlated insulating states and superconductivity is recently observed for a so-called magic-angle twisted bilayer graphene. Furthermore, beyond graphene, other 2D materials, such as silicene, phosphorene, and the recent black phosphorus /MoS_2 heterojunctions, which are 2D allotropes of bismuth and antimony grown on highly ordered pyrolytic graphite and MoS_2, are considered. Finally, the optically important exciton phenomenon, which depends on the moiré potential and has been observed for a moiré superlattice of transition metal dichalcogenides, is discussed. This overview aims to cover all the fascinating prospects that depend on the moiré superlattice, ranging from electronic structure to optical exotics among flatland materials.

1. Introduction

For almost two decades layered materials have proven themselves to be fascinating building blocks for advanced materials engineering. These materials with their intrinsic van der Waals (vdW) coupled stacks of 2D atomic sheets exhibit novel properties distinct from those of their bulk counterparts. This exotic flatland regime of materials has triggered rapid advancements ranging from fundamental physics to device applications.[1,2] Research in layered materials started with the one-atom-thick carbon allotrope graphene,[3] which has since grown into a family of 2D crystals covering all types of electronic structures including metallic, semiconducting, and insulating flatland domains.[2,4] Every year thousands of papers dedicated to graphene-based materials are published. Interlayer vdW coupling in 2D crystals allows the electronic properties to be flexibly tuned. Among the methods that are available for electronic structure tuning, one straightforward approach is contrived from the stacking sequence.[5–7] Different stacking arrangements can be achieved by relying on the weak vdW interactions, which provide extended freedom for an even greater variety of interlayer twist angles. The twisted layer structures that were first observed for graphene grown using chemical vapor deposition (CVD) are now readily achieved by direct growth, such as by using controlled transfer fabrication techniques. Recent reports have revealed the role of vdW coupling in the growing family of flatland materials.[8,9] From an applications point of view, new pathways have been explored to develop high-performance electronic,[10–12] photovoltaic,[13] photonics and optoelectronic devices,[14–54], e.g., field-effect transistors[55] and light-emitting

Dr. G. Abbas, Dr. Y. Li
College of Materials Science and Engineering
Shenzhen Key Laboratory of Special Functional Materials
Shenzhen Engineering Laboratory for Advanced Technology of Ceramics
Guangdong Research Center for Interfacial Engineering of Functional Materials
Guangdong Provincial Key Laboratory of Deep Earth Sciences and Geothermal Energy Exploitation and Utilization
Shenzhen University
Shenzhen 518060, China
E-mail: liyu@szu.edu.cn

Dr. G. Abbas, Dr. W.-X. Zhang
School of Materials Science and Engineering
Hanshan Normal University
Chaozhou 521041, China

The ORCID identification number(s) for the author(s) of this article can be found under https://doi.org/10.1002/adfm.202000878.

Dr. G. Abbas, Dr. H. Wang, Dr. C. Wang, Prof. H. Zhang
Institute of Microscale Optoelectronics
International Collaborative Laboratory of 2D Materials for Optoelectronics Science and Technology
Key Laboratory of Optoelectronic Devices and Systems of Ministry of Education and Guangdong Province
College of Physics and Optoelectronic Engineering
Shenzhen Key Laboratory of Micro-Nano Photonic Information Technology
Guangdong Laboratory of Artificial Intelligence and Digital Economy (SZ)
Shenzhen University
Shenzhen 518060, P. R. China
E-mail: hzhang@szu.edu.cn

DOI: 10.1002/adfm.202000878

 © 2020 WILEY-VCH Verlag GmbH & Co. KGaA, Weinheim

diodes.[56–59] Moreover, 2D materials and their vdW heterostructures have been widely used in energy,[60–62] catalysis,[63–68] sensing,[69] biomedicine,[70–76] memristive devices[77–80] and so on. However, recent flatland materials have witnessed new development contrived from their interlayer twist angles. This has been proven to be a highly unique way to temper conventional electronic structures to attain unexpected electronic states in materials with flat structures.[5,81]

Overlaying two sheets with mesh produces a panoply of well-known moiré patterns with beautiful interference. For centuries, artists have been playing with this technique to produce textures and shapes that are visually attractive. This craft has found its way into advanced 2D material science, where identically similar 2D bilayers, upon being twisted (i.e., rotated) with respect to each other, change their periodic potential to form moiré electronic superlattices.

Distinctively different from pristine ground state bilayer crystals, the electronic properties of moiré crystals are sensitive with respect to the interlayer coupling strengths. These electronic structures can easily be understood with perturbation theory;[82] however, for some special twist angle now termed the magic angle, the explanation is not that simple. In particular, in the case of graphene, when the bilayer twist angle is smaller than 2°, the electronic structure becomes much more complex with the appearance of flat bands with unexpected states. In the recent most decade, the twist in the stacking sequence has been shown to be strongly coupled to diverse physical parameters via interlayer interactions.[1,83–91] This opens up an entirely new realm to explore the novel physics linked to the electronic structure produced as a result of the critical stacking sequence of vdW-coupled bilayers. Normally, a graphene bilayer with free electrons deviates from the norm to produce exotic new physical properties around these twisted magic angles. For example, a Mott insulator and unconventional superconductivity were unexpectedly observed for the first time with graphene twisted at a small magic angle because of electron localization within the moiré superlattice.[83,84,92]

These new developments in the past decade have set the stage for the advent of twistronics.[82,89,93–97] Researchers have taken advantage of the relative twist angle and flat bands to craft moiré superlattices as a new way of altering the electronic structure to tailor the properties of devices based on 2D materials, which are rapidly expanding into a family of available 2D building blocks. As such, collections of materials from which to select options for crafting vdW-coupled heterostructures is central to a variety of materials systems. Apart from this diversity, twistronics allows this very new realm of physics to be brought to center stage.

Here, we review novel physical insights into the electronic structure of the twisted bilayer graphene moiré superlattice, along with the highly correlated unprecedented physics associated with the magic angle and the potential of tailoring the properties for electronic device applications. In addition, we consider 2D materials beyond graphene, such as silicene, phosphorene, and transition metal dichalcogenides (TMDCs). Our review attempts to cover all new breakthroughs in the physics of interfacial moiré patterns generated as a result of lattice mismatch or engineering of the interlayer twist angle. Finally, we provide the outlook for prospective vdW-coupled twistronic materials in future generations of electronic devices.

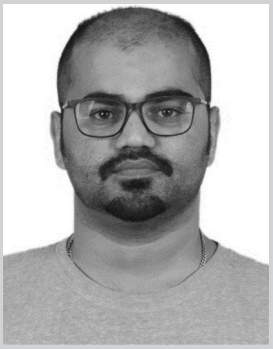

Ghulam Abbas, originally from Pakistan, completed his Ph.D. in 2019, from University of Science and Technology China. He is now working as postdoc under the joint program of Shenzhen University, Shenzhen and Hanshan Normal University, Chaozhou, Guangdong Province, China. His current research interests involve designing novel low-dimensional materials by understanding their atomistic-level properties through electronic-structure theory in combination with first-principles calculations.

Yu Li received her B.S. degree from Shandong University in 2008 and her Ph.D. degree from the University of Science and Technology of China (USTC) and City University of Hong Kong in 2013. She is currently a director of the Shenzhen Key Laboratory of Special Functional Materials, and the College of Materials Science and Engineering, Shenzhen University. Her research focuses on designing, fundamental study, and applications of optoelectronic, thermoelectric 2D materials and layered crystals, in combination with first-principles calculations.

Han Zhang received his B.S. degree from Wuhan University in 2006 and his Ph.D. degree from Nanyang Technological University in 2010. He is currently a director of the Shenzhen Key Laboratory of 2D Materials and Devices, and the Shenzhen Engineering Laboratory of Phosphorene and Optoelectronics, Shenzhen University. His current research focus is ultrafast and nonlinear photonics of 2D materials.

2. Crafting a Moiré Superlattice

From a structural point of view, an understanding of both real and reciprocal space projection for moiré patterns generated as a consequence of misalignments is crucial. Moiré patterns can arise under two conditions, either when the two lattices have slightly different parameters or when identical lattices are twisted at an angle θ with respect to each other. Here, we

© 2020 WILEY-VCH Verlag GmbH & Co. KGaA, Weinheim

first focus on the former, a typical graphene-like commensurate bilayer system, which is defined as the rotational change in lattice vector $\mathbf{V}(m, n)$ to $\mathbf{V}'(n, m)$ with n, m being the coordinates with respect to the basis vectors $a_1\left(\sqrt{3/2}, 1/2\right)$ and $a_2\left(\sqrt{3/2}, 1/2\right)$. The rotation angle is defined by the following relation[82]

$$\cos\theta = \frac{n^2 + 4\,nm + m^2}{2\left(n^2 + nm + m^2\right)} \tag{1}$$

where the commensurate cell vectors have the following correspondence

$$\vec{t} = \mathbf{V}' = n\vec{a}_1 + m\vec{a}_2;\ \vec{t}' = -m\vec{a}_1 + (n+m)\vec{a}_2 \tag{2}$$

This allows us to derive the following important points about this superlattice[82,98,99]

i. The commensurate unit cell contains $N = 4(n^2 + mn + m^2)$ atoms.
ii. For $\theta \approx 0°$, a large cell with large n and m and small $|m - n|$ is obtained, whereas large cells can also form $\theta \approx 30°$, in which case $|m - n|$ is large as well.
iii. For $c = 60°$ perfect AB stacking sequences are obtained, and for $n = 1$ ($m = 1$) and large m (n), θ approaches 60°.
iv. For a smaller angle of rotation θ, a periodic supercell is obtained with all types of perfect stacking arrangements (AA, AB, and BA) appearing diagonally, as shown in **Figure 1**.

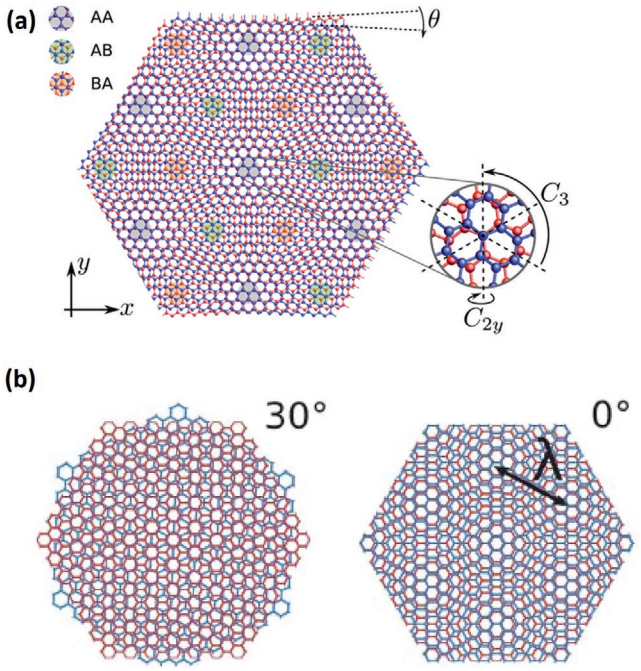

Figure 1. Moiré superlattice formed under either commensurate or incommensurate bilayers. a) Bilayer graphene moiré superlattice with an interlayer twist angle θ. For bilayer graphene, regions of local AA, AB, and BA stacking are highlighted as gray, green, and orange regions. The generators of the point group D_3 of the system are illustrated in the inset, where the twist angle θ has been chosen larger enough to make the geometry more visible. Reproduced with permission.[100] Copyright 2018, American Physical Society. b) Graphene/BN sheets are highlighted as red and blue for graphene/BN systems; the moiré superlattice wavelength is also shown for zero twist angle system. Reproduced with permission.[85] Copyright 2018, American Association for the Advancement of Science.

Under the former condition, adjustment of the lattice length also results in moiré patterns, for example, those observed for hexagonal boron nitride (hBN) and graphene heterostructures. This is because the slightly longer lattice lengths of hBN are already a moiré superlattice produced by an incommensurate layer and could be amended further by relative rotation,[87,101] as shown in Figure 1b. Such a moiré superlattice, for a given lattice mismatch δ between two stacked layers with a relative rotational angle φ, has a unique corresponding moiré superlattice wavelength, given as

$$\lambda = \frac{(1+\delta)a}{\sqrt{2(1+\delta)(1-\cos\phi)+\delta^2}} \tag{3}$$

where a is the lattice constant for graphene. The relative rotational angle θ with respect to the graphene lattice of the moiré pattern is given as

$$\tan\theta = \frac{\sin\phi}{(1+\delta)-\cos\phi} \tag{4}$$

The lattice mismatch produces moiré patterns for all the orientations of graphene over hBN.[102] Several techniques to fabricate stacked layered structures are known. However, recent developments in highly sensitive moiré physics require more careful control over the relative twist angles of the interlayer. Methods that are generally employed to achieve such relative twisted layers are nondynamic; in other words, once the bilayer has been twisted, the superlattice cannot be subjected to any further twist improvisations. In Section 2.1, we review the main fabrication techniques and, more importantly, recent achievements in terms of controlling the angles of a moiré superlattice. Along with more advanced improved methods, we present techniques that were developed to fabricate devices based on dynamic interlayer twisting angles.

2.1. Fabrication Techniques

The burgeoning development of the field of moiré superlattice fabrication demands very high control over fabrication techniques to obtain the desired interlayer twist among flatland moiré superlattices. A summary of the more recently improved fabrication techniques is given below.

2.1.1. SiC-Based Epitaxial Growth

One of the first twisted bilayer graphene samples was actually observed for SiC-based epitaxial growth. However, since then it became clear that the efficiency of this method was insufficient to fulfill research and practical needs. This is because the number of layers, the size of samples, and more importantly, the interlayer twist angle could not be controlled. However, scanning tunneling microscopy (STM) analyses of samples grown by using epitaxial growth in all studies of graphene fabrication revealed the formation of a twisted bilayer graphene superlattice as shown in **Figure 2**.[5,103–105]

© 2020 WILEY-VCH Verlag GmbH & Co. KGaA, Weinheim

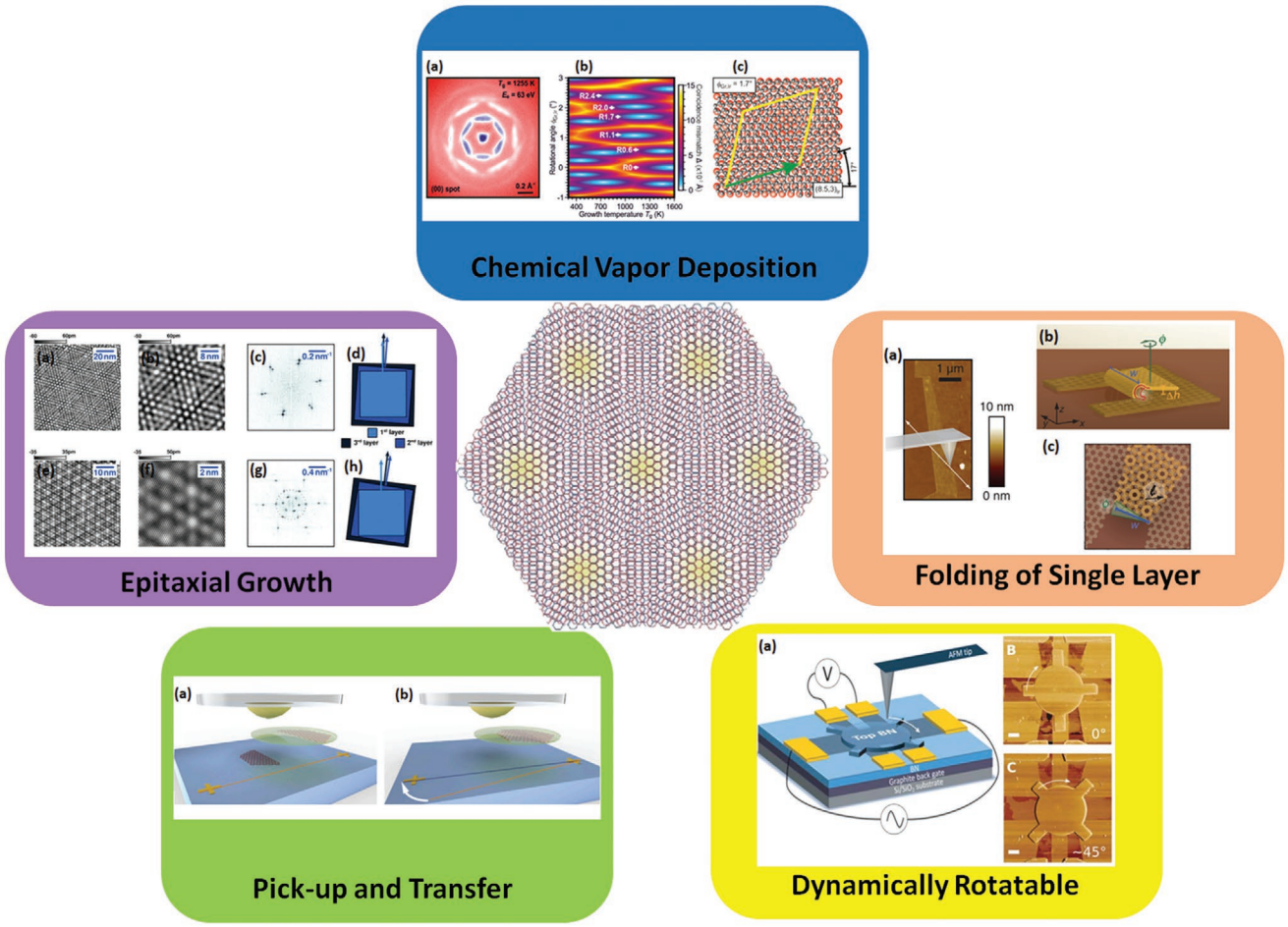

Figure 2. The collage summarizes the available fabrication techniques for moiré superlattice. The purple box contains images of STM topographs of multilayer twisted epitaxial graphene, in which (a) and (e) are for two similar- and disimilar-interference moiré patterns for a large supercell, along with zooms b,f), Fourier transforms c,g), and schematics of the layer orientations d,h). Images in the purple box: Reproduced with permission.[104] Copyright 2010, American Physical Society. The green box shows device schematics implemented to achive twisted bilayer fabrication from single-layer graphene sheets a,b). Images in the green box: Reproduced with permission.[94] Copyright 2017, National Academy of Sciences. The blue box shows chemical-vapor-deposited moiré patterens: a) Spot profile analysis–low-energy electron diffraction, b) 2D representation of the coincidence mismatch Δ as a function of the rotational angle $\phi_{Gr,Ir}$, and c) real-space model of the moiré superstructures' growth over an Ir(111) surface. Imaegs in the blue box: Reproduced with permission.[114] Copyright 2019, American Chemical Society. The orange and yellow boxes contain two very new developments, one-base one-single-sheet Atomic Force Spectroscopy (AFM) controllable folding is shown in the orange box. Reproduce with permission.[112] Copyrights 2019, IOP Publishing. Schematics of a device for achieving rational dynamic 2D heterostructures, along with AFM images are, shown in yellow box. Reproduce with permission.[89] Copyrights 2018, American Association for the Advancement of Science.

2.1.2. Chemical Vapor Deposition

CVD[22] has evolved over the years as a widely used reliable method for the production of graphene sheets on a substantial scale.[106,107] In addition, bilayer domains are also formed, ranging from a few micrometers to as many as dozens of micrometers in size.[108] Irrespective of the superior quality of graphene obtained via CVD, the method still does not allow the fabrication of multilayer angular graphene sheets. However, the preparation of twisted graphene by CVD methods is relatively easy. These methods were also found to be useful for producing commensurate TMDC with a twisted bilayer moiré superlattice.[109] Very recent methods demonstrated that variation of the Ir (111) substrate temperature during the growth of graphene can be used to obtain distinct relative rotational angles of 0°, ± 0.6°, ± 1.1°, and ± 1.7° as shown in Figure 2. These growth methods based on rotational epitaxy may provide a route to achieve particular orientations in the stacks of 2D materials, and, thereby, unique material properties are achieved.[110]

2.1.3. Folding of Single-Layer Graphene

The first graphene flakes were obtained by using mechanical exfoliation techniques.[3] For the purpose of scientific investigations, this method provides high-quality graphene samples ranging from a few micrometers to more than a dozen micrometers. Even though these methods usually have a low sample yield, folding can be used to produce an uncontrolled single interlayer twist angle and, consequently, a graphene moiré superlattice.

© 2020 WILEY-VCH Verlag GmbH & Co. KGaA, Weinheim

Although this method offers an easy way to a moiré superlattice, it also limits systematic control over the twist angles, according to studies that aimed to reveal the effect of these angles on the performance of a twisted bilayer system. However, recent improved folding techniques suggest that an understanding between the orientation of the folding sheets and the stacked twisted angles could facilitate the fabrication of tailored moiré patterns.[111] One such method shows that graphene can be made to grow under such a folded superlattice. The growth seed could be induced by scratching a graphene flake carefully with atomic force microscopy (AFM) nanomachining to create an additional surface with rough edges. Such artificial perturbations are prone to fold-overs (Figure 2); alternatively, this could be achieved by simply using contact-mode tracing of an actual flake edge.[112]

2.1.4. Pick-Up and Transfer

Modern techniques, such as a high-energy femtosecond laser could be used to precisely slice off a freshly exfoliated single layer of graphene over SiO_2/Si substrates into two straight pieces. This, in combination with a custom transfer technique, could further improve control over the stacked interlayer twisting angles to obtain 0.1° precision.[113] Such a controlled pick-up and transfer method was demonstrated by Kim et al., who showed that the method relies on detaching a microsized sample from the substrate with the help of a semispherical shape produced from polyvinyl alcohol-coated epoxy. That is, lateral movement is used to separately detach two single-layer sheets from the surface of the SiO_2/Si substrate and these sheets are placed over one another to form a heterostructural region in between as also illustrated in Figure 2.[94]

2.1.5. Dynamically Rotatable Heterostructures

A recent advancement is the development of a dynamic rotatable heterostructural device by Ribeiro-Palau et al. Several techniques, as discussed above, allow the rotational angle of structures to be controlled; however, prior knowledge of the crystallographic orientation is essential for all these methods. Moreover, once the rotational angle has been set, further alteration during experimental analysis is not possible. This rules out sample-to-sample variation in a systematic study of the effects of the twisted angle.[115] Dynamical relative rotation between stacked bilayers is advantageous in that it allows significant freedom over otherwise static fabrication techniques.[89] Ribeiro-Palau et al. demonstrated graphene encapsulated with BN as a device with tunable twist. The layers of this tri-layer can be rotated relative to one another to fabricate a novel dynamical device. Moreover, the approach is expected to be easily extendable to the fabrication of generic heterostructures from a variety of 2D materials. Furthermore, the ability to tune the band structure and controlling the extent to which superconductivity depends on the twist angle may be exploited to control a Mott-like insulator by varying the rotation of the layers.

To summarize the above, each technique possesses a unique outcome for moiré superlattice fabrication. As mentioned, epitaxial growth methods have become insufficient to fulfill the demand, and also lack control over whole fabrication outcomes. However, techniques like folding over and pick-up and transfer are advancing toward the provision of much more control over the desired twist angle. CVD growth is more reliable for preparation of large quantities of a sample, which can now be used to fabricate dynamically rotatable devices of overlaid flatland materials producing moiré interferences. The collage in Figure 2 highlights advanced fabrication control over moiré superlattice in flatland materials. However, much still needs to be done to make careful fabrication of moiré superlattice structures a simple routine task for advanced functional materials sciences.

3. Graphene Moiré Superlattice

Carbon is the *materia prima* of all organic matter, mainly because of its versatile bonding ability. Apart from this, it has been extended to reveal many of its bonding configurations in its elemental allotropes, which have attracted considerable attention, and which have their respective unique physical properties that depend on various factors. These versatile physical properties mainly vary in their unique correspondence to the dimensionality of the different allotropic forms of graphene. From 0D fullerenes to 1D carbon nanotubes, 2D layers of graphene offer much more freedom with an sp^2-hybridized honeycomb network of carbon atoms. 2D materials show much more promise than 0D and 1D materials in the field of vdW interfacial engineering. This translates into exotic physical properties, such as excellent mechanical strength,[116–118] ultrahigh thermal conductivity,[119–122] and broadband light transmittance.[123–126] Thus, before providing more details we first discuss the elementary electronic structure of graphene, which we explain within the perturbation theory for electronic structures.

3.1. Typical Electronic Structure

The graphene monolayer lattice is formed by a hexagonal unit cell that contains two atoms of carbon. This arrangement results in interpenetrating triangular lattices, as shown in Figure 1a. Similar to a benzene ring, each of the sp^2-hybridized carbon atoms forms three σ-bonds with other in-plane neighboring carbon atoms, whereas the p_z-orbital forms more dispersed π-bonds. Overall, π-bonds are mainly responsible for the characteristic dispersion of bands with a conical shape around the zero energy points K and K′ (Dirac Points, Figure 2b,c), which are also responsible for novel semimetallic electronic and physical properties. From a dimensionality point of view, the electronic structure of graphene differs from that of carbon nanotubes, where 1D band folding leaves carbon nanotubes either metallic or semiconducting with respect to the folding sequence and resulting in much denser density of states with van Hove singularities.[127,128]

3.2. Bilayer Electronic Structure

As the number of layers increases, the electronic structure starts to vary under the influence of interlayer electronic coupling, and this also affects the properties. For a bilayer

© 2020 WILEY-VCH Verlag GmbH & Co. KGaA, Weinheim

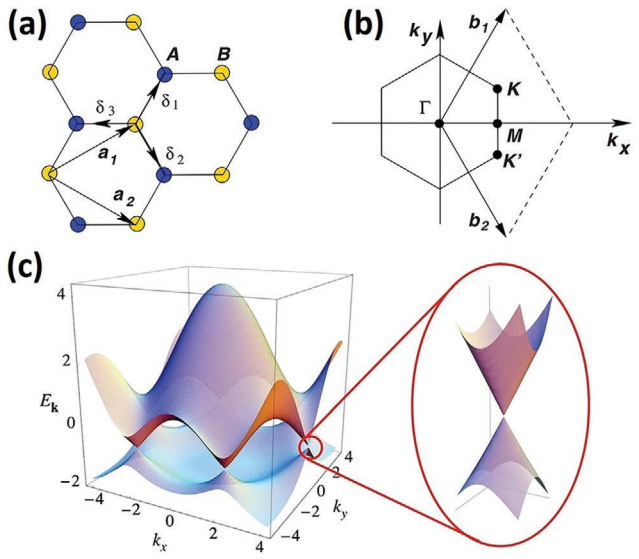

Figure 3. a) Honeycomb lattice of graphene formed by two interpenetrating triangular lattices, with a_1 and a_2 being the lattice unit vectors. b) Brillouin-zone lattice structure with corresponding Dirac cones are located at the points K and K′. c) Electronic dispersion in the honeycomb lattice with the energy spectrum and an enlargement of the energy bands close to one of the Dirac points. a–c) Reproduced with permission.[234] Copyright 2009, American Physical Society.

system, interlayer hopping modifies the band structure of the π-bands, which are energetically at very similar levels. The linearly dispersed degenerate π and π^* bands split into four nearly parabolic bands. The electronic properties of graphene bilayers are generally interpreted in terms of AB-type stacking, which refers to the energetically favored AB-type or Bernal stacking sequence for bilayer graphene. An AB-type bilayer system has the carbon atoms in the second layer located at the center of a hexagon in the first layer, as shown in **Figure 3**c. A small gap of a few meV can be opened by application of an electric field perpendicular to the 2D plane (Figure 3d) for the valence and conductance bands of otherwise isolated gapless bilayers, which is promising for field-effect transistors.[129–135]

Overall, despite considerable research effort, the performance is still not sufficiently satisfactory for logical applications, mainly because of the many defects related to the stacking sequence. In the case of the energetically less favorable AA-type stacking, the system remains a gapless semimetallic system. Under ordinary conditions, AA stacking with domains that contain imperfections allows conductive pathways and diminishing bilayer graphene field-effect transistor performance. Apart from AA- and AB-type stacking, the layers comprising a bilayer structure could be mutually twisted, in which case the C—C bonds of neighboring layers are rotated with respect to each other by a certain angle ($0° < \theta < 180°$). Stacking sequences such as these are directly achieved by CVD growth,[136–141] mechanical exfoliation,[130,132,142] or special transfer techniques.[129,143–145]

3.3. Twisted Bilayer Graphene

The twisted layers in bilayer graphene contribute to making the electronic structure too intriguing and complex to explain by way of the simple perturbation theory of electronic structure. Twisting leads to the formation of moiré patterns with long periods as illustrated in **Figure 4**a. In this case, the two

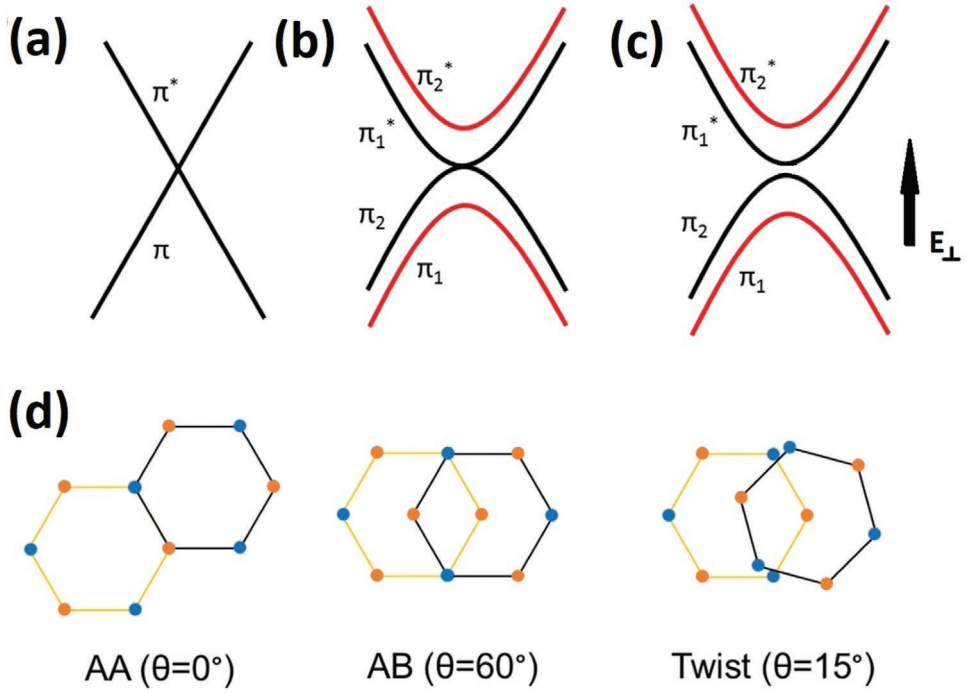

Figure 4. a–c) Illustration of electronic band for structure of monolayer a) and AB-stacked bilayer b) graphene along with band opening under an applied out-of-plane electric field E for AB-stacked bilayer graphene c). d) Lattice configurations of AA-stacking, AB-stacking, and twisted bilayer graphene. Reproduced with permission.[236] Copyright 2017, Wiley-VCH.

© 2020 WILEY-VCH Verlag GmbH & Co. KGaA, Weinheim

Dirac cones couple via periodic interactions within the larger supercell, restoring linear band dispersions that are absent from the Bernal stacking of graphene. These Dirac cones were experimentally observed for 11 layers stacked over the carbon face of SiC,[146] and these sheets showed transport properties highly similar to those of isolated graphene. This was mainly attributed to twist defects that normally remained unaddressed in early studies carried out on graphene bilayers or multilayer systems.

Subsequent theoretical studies were conducted to explain the orientational disorder observed in experiments.[147,148] These studies not only confirmed the peculiar experimental observation of multilayer orientation disorder in graphene stacks,[104,149] they also showed that the Dirac cones were preserved as in a single layer but the Fermi velocity was reduced significantly, especially for rotations at a smaller angle.[82,99] At the point at which the Dirac velocity was shown to cross the zero level several times, as shown in Figure 4c, for a certain magic angle the moiré band actually flattens and the two layers become more strongly coupled.[99,149]

The first moiré superlattice in graphene, which formed the topic of an in-depth investigation, was discovered to exist in CVD grown flakes of graphene.[5] In bilayer twisted graphene systems, the characteristics of the Dirac points distinctively differ from those of the pristine single-layer constituents. In these twisted layers, the Dirac cones separated by ΔK make contact with each other, and form two new saddle points in the positive and negative energy regions, contributed by the upper and lower layers, as shown in Figure 6a. These electronic modulations are imaged as two pronounced distinct high-density states around the Fermi level as van Hove singularities (VHS).[151] Their appearance around the Fermi level makes these singularities much more interesting, as they could be regulated or even made to coincide with the Fermi level to form flat bands at the magic twist angle ($\theta \approx 1°$) as shown in **Figure 5**c. Their dependency on the rotational angle θ was also demonstrated both experimentally and theoretically, as shown in **Figure 6**b,c.[92,95,151–153] These features were recently exploited to achieve exotic properties for very small angle twisted bilayer graphene moiré superlattice structures.[88] The relationship of the VHS separation to the twist angle θ was derived and is expressed in the form of an empirical formula

$$\Delta E_{\mathrm{VHS}} = \hbar v_{\mathrm{F}} \Delta K - 2t_{\theta} \tag{5}$$

where $\Delta K = 2K \sin\frac{\theta}{2}$, v_{F} is the renormalized Fermi velocity, and t_{θ} is the interlayer hopping energy.

At large twist angles, the crossing energy is sufficiently far from the Dirac point and physics of the low-energy part of the Dirac cones is indistinguishable from that of a single layer. However, for very small angles ($\theta > 3$) modifications occur, in which case the Fermi v_{F} renormalization is given as[154]

$$\frac{v_{\mathrm{F}}^{\theta}}{v_{\mathrm{F}}^{0}} = 1 - 9\left(\frac{t_{\perp}^{\theta}}{\hbar v_{\mathrm{F}}^{0} \Delta K}\right)^{2} \tag{6}$$

For Bernal stacking, where $t_{\perp}^{\theta} \approx 0.4t$, it was found that for very small twist angles the Fermi velocity is not only dependent on the twisting angles as shown in **Figure 7**a, but also on interlayer coupling. This is accompanied by discreet Landau-level quantization of Dirac massless fermions.[155] The discreet Hofstadter butterfly spectra are also shown in Figure 7b.

3.4. Magic-Angle Moiré Superlattice

In the last two years, twisted bilayer graphene has undergone unprecedented developments specifically related to so-called "magic angle" twisted bilayer graphene. As mentioned above, the existence of moiré bands between the layers of twisted bilayer graphene was predicted theoretically almost a decade ago. For larger twist angles, it was shown that these bands arise when subjected to twist-modulated electronic tunneling between the two layers in a spatially periodic way, whereas for very small twist angles they are almost flattened when the modulation wavelengths become extremely long.[82,99,150] However, early studies remained unclear about the mechanism underlying the formation of these flat bands. Further details were subsequently revealed with the help of tight binding models,[156] such as that the flattening is not monotonic with respect to the twisting angles and the band only completely flattens for discrete twist "magic angles" as show in Figure 5c.[149] This is also strongly indicative that the generation of flat bands, only for discrete small angles, presents the opportunity to control strongly correlated electrons on demand. Cao et al. recently discovered unconventional superconductivity for such a strongly correlated magic-angle twisted bilayer moiré superlattice of graphene. In addition, this long-wavelength moiré superlattice had insulating states at half-filling, which was unforeseen in the absence of strong interlayer coupling. Thus, we first consider the former case first.

3.4.1. Insulator and Superconducting Phase Interplay

Above we discussed the need to renormalize the Fermi velocity for long-period moiré superlattices with smaller twist angles. The velocity almost equals zero for a so-called magic-angle (≈1.1°) twisted bilayer graphene system. In the samples prepared by Cao et al. with a twist angle of 1.08°, the flat bands start to behave as insulating states for half-fillings. **Figure 8**c shows schematics for the formation of such a flat band as a result of hybridization between the two stirring Dirac points at the magic angle. In Figure 8a, the mini-Brillouin zone path illustrates high symmetry lines around these hybridized Dirac points. The band structure (Figure 8b), calculated with an ab initio tight binding model from first principle calculations, accurately shows band flattening along the mini-Brillouin zone path. For such a system, Cao et al. showed that at carrier half-filling, the behavior of these bands is similar to that of Mott insulator states. Figure 8d shows the results of tests that were performed to assess the conductive performance of such a system. The Dirac point is located at $n = 0$. The lighter-shaded regions are superlattice gaps at carrier density $n = \pm n_{\mathrm{s}} = \pm 2.7 \times 10^{12}$ cm^{-2}. The darker-shaded regions denote half-filling states at $\pm n_{\mathrm{s}}/2$. The inset shows the density locations of the half-filling states in four different devices. These Mott-like insulator states at the half-filling points are expected to be due to strong electron–electron Coulomb interactions.[157,158]

© 2020 WILEY-VCH Verlag GmbH & Co. KGaA, Weinheim

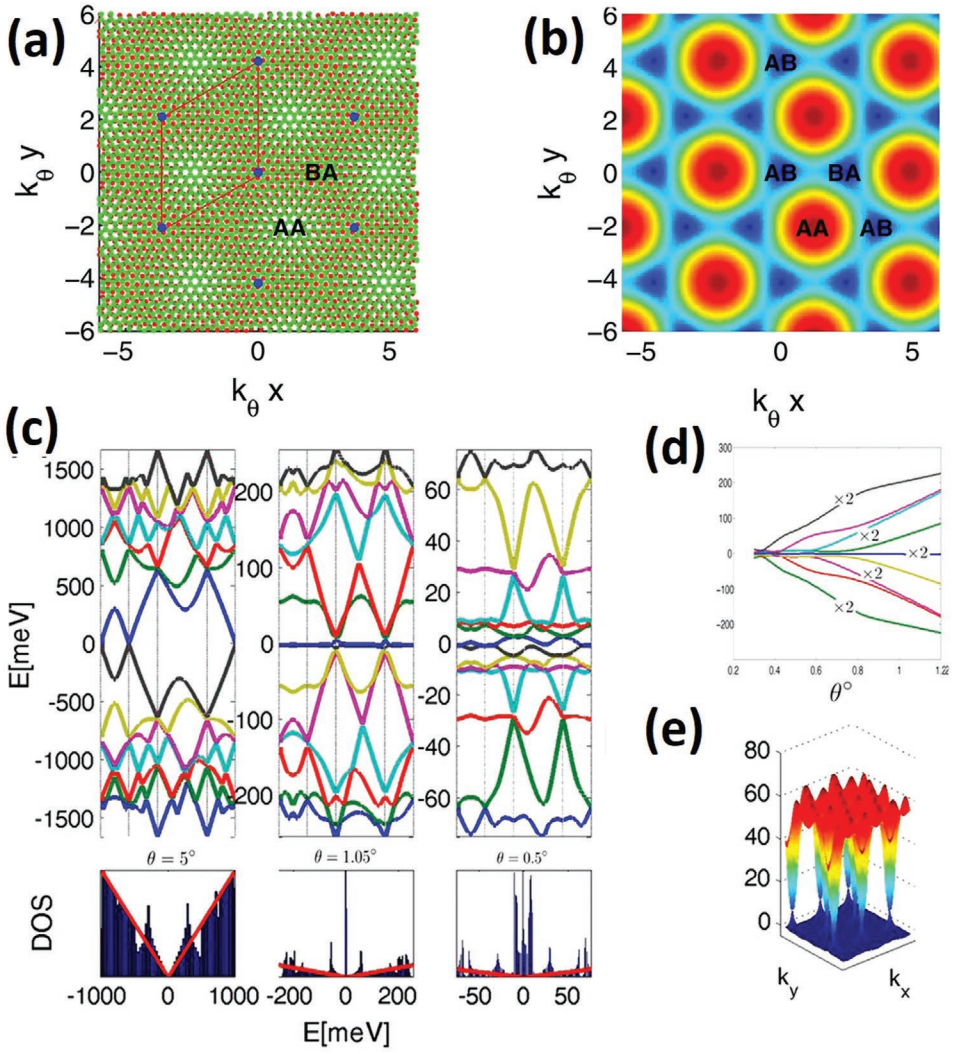

Figure 5. a) Graphene bilayer superlattice along with unit cell highlighted by red lines. b) Form the red to blue region, as we move along the moiré pattern, a maximum energy can be seen at AA, gradually vanishing at AB or BA stacking domains. Distances are measured in units of k_θ^{-1}, where $k_\theta = 2k_D\sin(\theta/2)$ with k_D being the Dirac wave vector. c) Moiré bands: Energy dispersion for the 14 bands closest to the Dirac point plotted along the k-space trajectory A → B→ C → D → A for w ¼ 110 meV, and θ ¼ 5° (left,), 1.05° (middle), and 0.5° (right) and DOS (bottom). d) Energy as a function of twist angle for the k ¼ 0 states. Band separation decreases with θ as also evident from in band structures. e) Full dispersion of the flat band at $\theta = 1.05°$. a–e) Reproduced with permission.[149] Copyright 2011, National Academy of Sciences.

In another research thread of Cao et al., they achieved zero resistance current for an electrostatically doped ≈1.1° "magic-angle" twisted graphene moiré superlattice of which the periodicity ≈13 nm. This happened to be an unprecedented breakthrough, namely the unexpected discovery of superconductivity in magic-angle twisted bilayer graphene. The question that remains is whether the insulating states observed for the twisted bilayer system promote the observed superconductivity. The answer is not straightforward; one exotic possibility is that both are mutually dependent. In a special case, the strongly interacting quasiparticles, which move in a correlated-electron environment, favor an insulating state locally. An example thereof is found in cuprates, which exhibit superconductivity at significantly higher temperatures.[159,160] Although the phenomenon could not yet be explained, further details may be revealed by studying magic-angle twisted graphene moiré superlattices. A specific connection scientists have succeeded in establishing between the two phenomena is the moiré filling factor "ν_m" (i.e., the fraction of filled states in a given band), which is an electronically tunable factor. **Figure 9**a shows the original four-probe device Cao et al. used to study superconductivity in twisted bilayer graphene with a very small angle. Figure 9b shows the measured resistivity for two different devices with slightly different twist angles. The device labeled M2 with a twist angle of 1.05° clearly shows zero resistivity at a temperature of ≈1.7 K, confirmation of superconductivity. Figure 9c is an illustration of two correlated insulating and superconducting states in proximity of one another, which is also similar to a cuprate superconductor as a function of ν_m.[161] This property is tunable via electronic gate implementation and the tuning

© 2020 WILEY-VCH Verlag GmbH & Co. KGaA, Weinheim

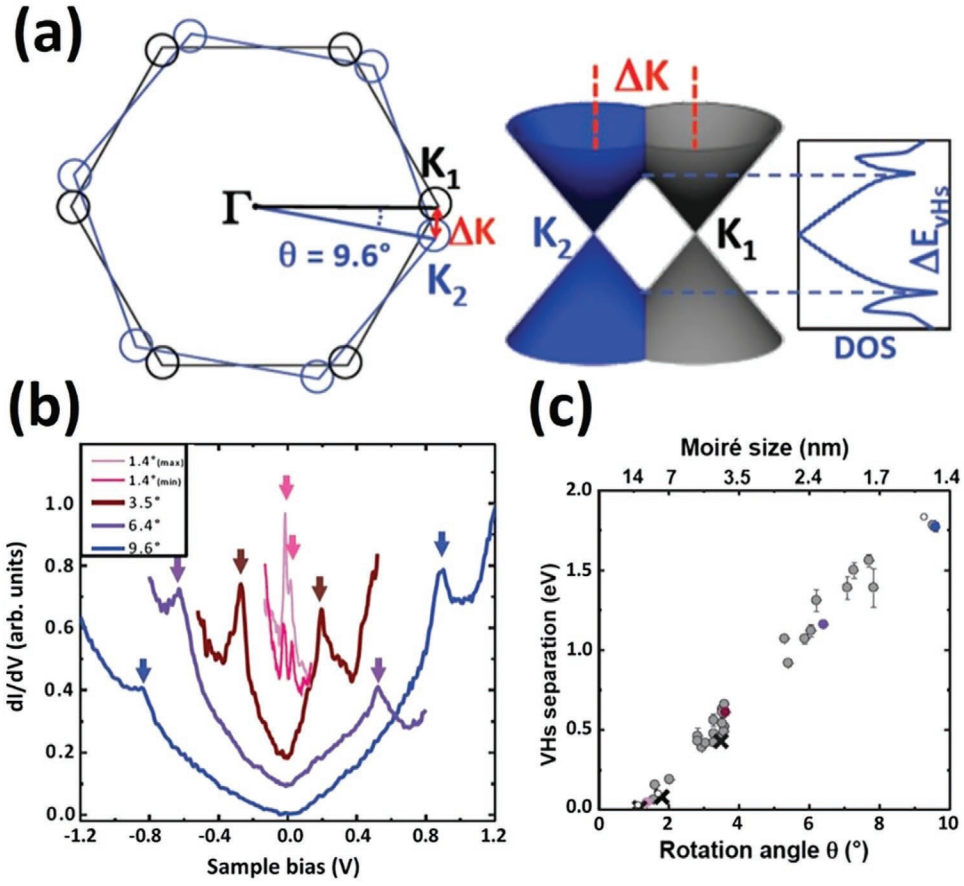

Figure 6. a) Illustration of mini Brillouin zone path for twisted bilayer graphene along with touching Dirac cones and how these form saddle point around Fermi level. b,c) The LDOS for moiré pattern and its variation along with plot of moiré pattern VHS separation energy as a function of change in twist angles. a–c) Reproduced with permission.[151] Copyright 2012, American Physical Society.

experiments also revealed that insulating states occur at most integer values of ν_m, whereas, as far as superconductivity is concerned, it occurred at ν_m close to, but not equal to, an integer (Figure 9c).

3.4.2. STM/STS of Magic-Angle Twisted Bilayer Graphene

As shown and discussed in Section 3.4.1, magic-angle twisted bilayer graphene exhibits two totally different phases at different

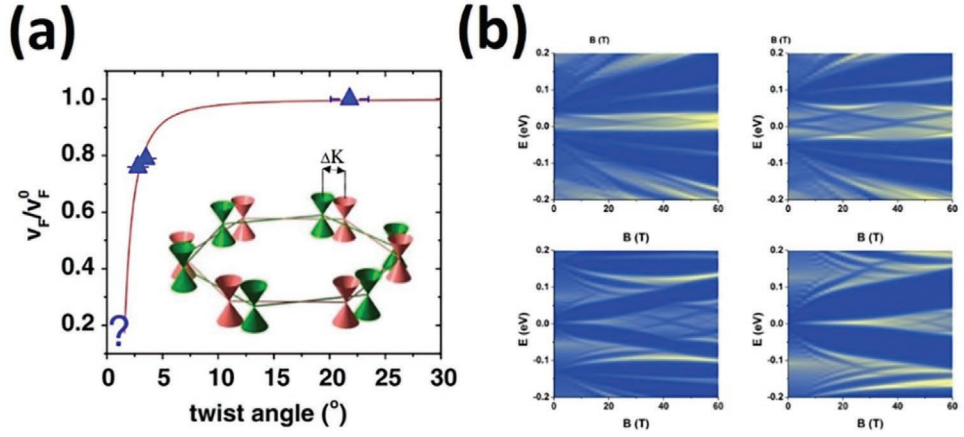

Figure 7. a) Angle dependence of Fermi velocity renormalization. Reproduced with permission.[154] Copyright 2011, American Physical Society. b) Hofstadter butterfly spectra of twisted bilayer graphene in the intermediate-coupling regime at a few selected twist angles. The top row in (b) is for commensurate angle $\theta = 1.067°$ and incommensurate angle $\theta = 1.3°$, whereas the bottom row is commensurate angle $\theta = 1.872°$ and incommensurate angle $\theta = 2.5°$. Reproduced with permission.[155] Copyright 2012, American Chemical Society.

© 2020 WILEY-VCH Verlag GmbH & Co. KGaA, Weinheim

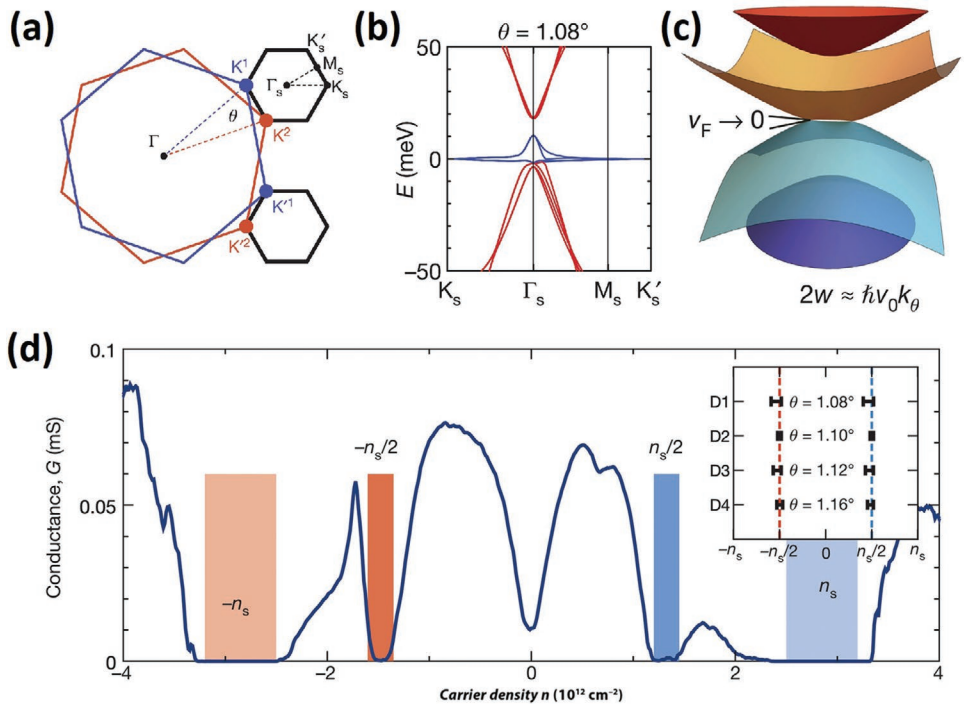

Figure 8. Electronic structure along with conductance plot for twisted bilayer graphene. a,b) Mini Brillouin zone path a) along the corresponding electronic band dispersion b). c) Illustration for interlayer Dirac point hybridization. d) Measured conductance G of magic-angle TBG device with $\theta = 1.08°$ and T = 0.3 K. a–d) Reproduced with permission.[83] Copyright 2018, Springer Nature.

levels of electronic charge densities, a superconductive and an insulating phase, as shown in Figure 9c. Although conductivity studies were highly informative in this regard,[83,84] much of this very new correlated physics behind the magic-angle moiré superlattice of bilayer graphene still needs to be explained. This intriguing interlayer coupling and unexpected correlated phase

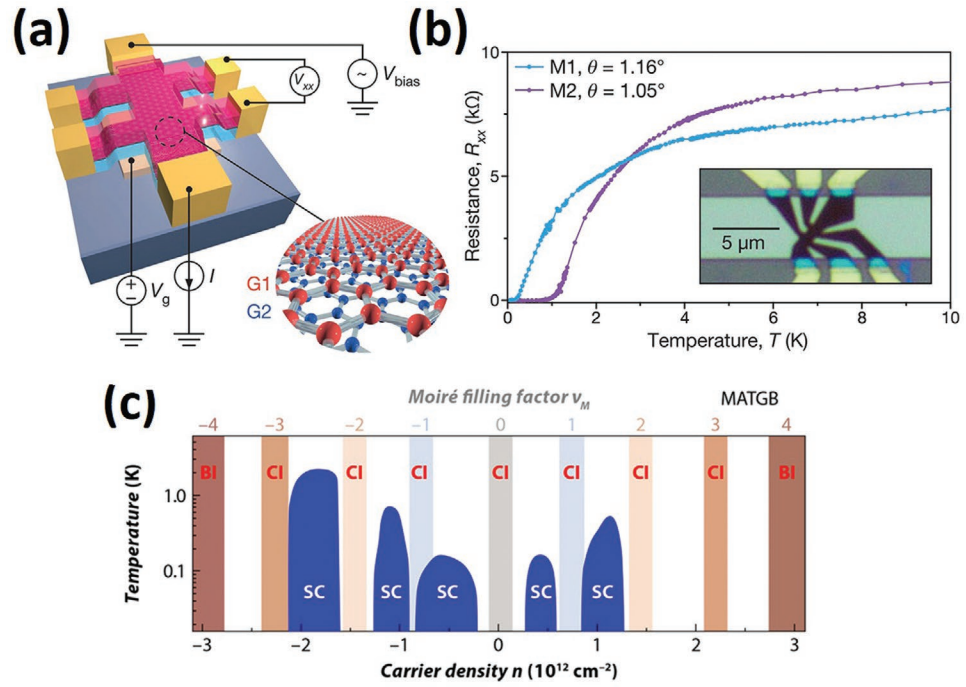

Figure 9. a,b) Schematic design of four probe fabricated device for measuring superconductivity in a magic-angle twisted graphene moiré superlattice a), along with measured resistivity plot with an inset optical image of device M2 b). a,b) Reproduced with permission.[84] Copyright 2018, Springer Nature. c) The schematic illustration of strongly correlated insulating (CI) and superconducting phases as a function of moiré factor. Reproduced with permission.[161] Copyright 2019, American Physical Society.

© 2020 WILEY-VCH Verlag GmbH & Co. KGaA, Weinheim

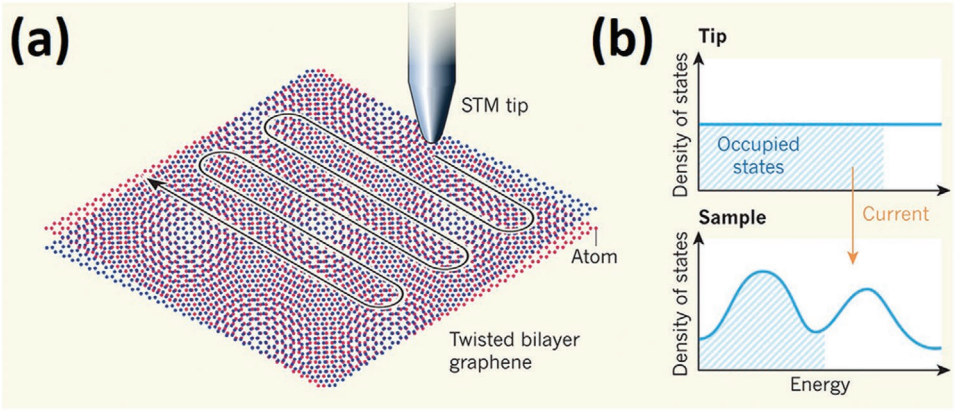

Figure 10. a,b) Schematic illustration for STM tip scanned across moiré superlattice a), along with density of states shown for both tip and sample b). When a voltage is applied (not shown), the values start to shift with respect to each other, as moving along electrons start to "tunnel" between the tip and the sample. Under the tunneling effect, a recordable electric current is produced. The number of states in the tip at a given energy its density of states is independent of the energy. Therefore, the variation in the current as function of voltage varies proportional to the density of states (DOS) of scanned sample. a,b) Reproduced with permission.[166] Copyright 2019, Springer Nature.

in magic-angle moiré patterns has ignited scientific intuition. Recent STM and scanning tunneling spectroscopy (STS) techniques were employed to directly visualize the local density of states to obtain deeper insights and find new pieces of the puzzle in an attempt to understand magic-angle moiré superlattices of graphene.[162–165] While we were preparing this review, four major relevant studies surfaced. Each of these studies presents key highlights to be noted along with certain discrepancies between them.[166] These results raise many new questions that have yet to be answered to enable a complete understanding of the exotic unexpected electronic correlated phase of graphene with a magic-angle moiré superlattice.

These studies relied on the techniques of STM and STS to reveal topographic information about the local density of states at the surface of the twisted bilayer sheets. The surface was studied by scanning a sharp tip, to which voltage was applied, across the surface, and, depending on whether the voltage is positive or negative, electron tunneling occurs, thereby causing variation in the electric current as the surface positioning of the tip changes. Schematics of which are shown in **Figure 10**a,b.

The worked carried out by these teams reveals the spatial arrangements of the carbon atoms under twisted bilayer coupling strain.[163] These details are essential for the exact modeling of the moiré superlattice for such twisted bilayer systems. The parameters for the model can be extracted by carefully quantifying the variation between the moiré fringes in the twisted bilayers. A closely related STS analysis carried out by Jiang et al. showed that a magic-angle moiré superlattice exhibits a pseudogap phase at half-filling points and that it results in broken rotational symmetries, whereas completely filled or empty flat moiré bands do not display this behavior. Xie et al. used the same technique and established that the simple mean-field approach breaks down to explain the features observed for their local density of states (DOS) visualization by STM. In contrast, extended phenomenological extended-Hubbard-model cluster calculations, which are usually the first choice for highly correlated superconductors (e.g., cuprates), were sufficient to produce spectroscopically observed features.[165] Overall, these insightful investigations with STM/STS techniques provided valuable insights into the symmetry breakdown of the local unexpected electron correlation observed in magic-angle moiré superlattice graphene. However, further improvements in these techniques are expected to eliminate unexplained discrepancies observed between the studies carried out by different groups. For example, an improvement is expected by conducting STM studies at lower temperatures as this could shed new light on the relationship between contrasting superconducting and insulator states.

4. Beyond Graphene

The large perturbation of an electronic structure under twisted bilayers has been extended to a method for electronic structure tunability. In the recent literature, we noticed explorations of moiré superlattice patterns in materials beyond bilayer graphene, which reveal exotic new physical phenomena for electronic band engineering. The ability to strongly modulate low-lying electronic states around the Fermi level by varying the stacking rearrangements has been well established.[5,84,167] In Section 3, we comprehensively reviewed recent progress to control the moiré superlattice of graphene and all new physical insights relating to the crossover of Dirac cones and flat band formations near the so-called magic-angle attribute to the rotation of the Brillouin Zone. Below we discuss twisted bilayer superlattices beyond graphene and their potential ability to tune the electronic structure of 2D materials.

4.1. Silicene

Silicene also possesses Dirac fermion characteristics that have attracted an equal amount of attention parallel to graphene.[168–173] Interlayer coupling in silicene is much stronger, with STM studies supported by ab initio density functional theory (DFT) methods showing that a hybridized sp^2–sp^3

© 2020 WILEY-VCH Verlag GmbH & Co. KGaA, Weinheim

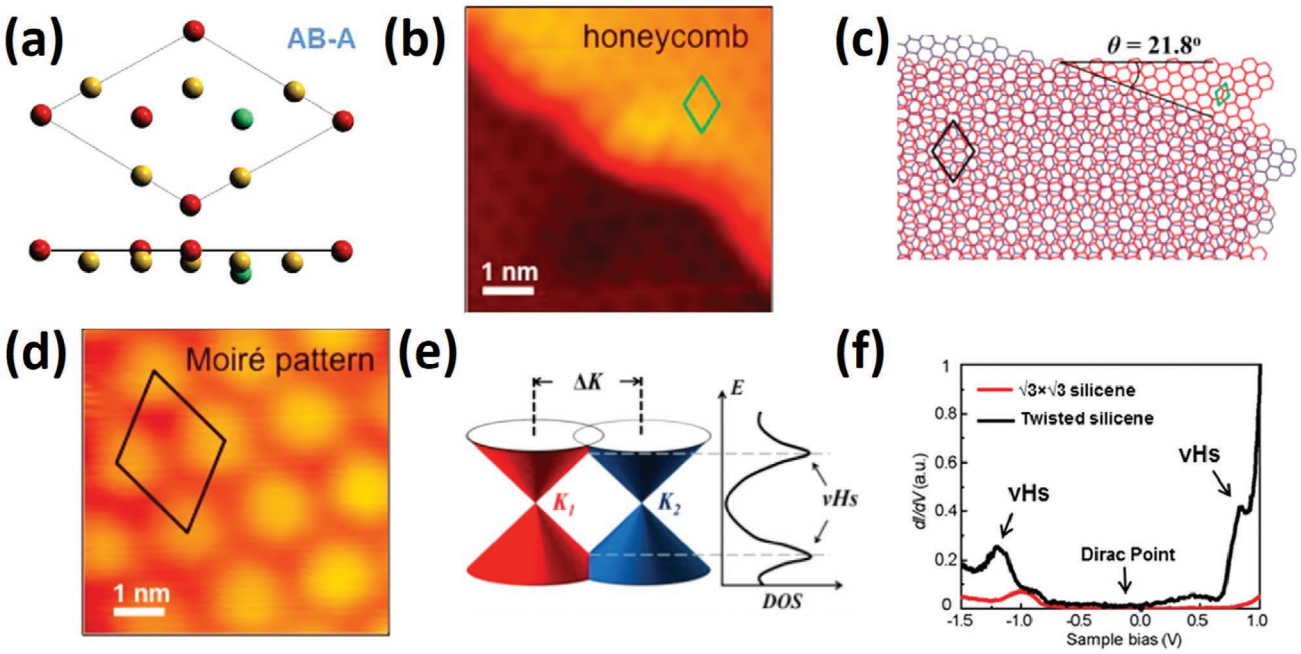

Figure 11. a,b) The $AB\bar{A}$ $\sqrt{3}\times\sqrt{3}$ unit cell of silicene along with STM image. a) Reproduced with permission.[170] Copyright 2012, American Physical Society. c,d) The moiré superlattice model for a twist angle of 21.8° along with STM observed periodic bright and dark regions of moiré patterns for a 1 nm unit across field of image. e,f) Illustration for symmetric formation of vHs on either side of the twisted Dirac points for bilayers along with experimental STS spectra clearly showing bumps for vHs. b–f) Reproduced with permission.[174] Copyright 2016, American Chemical Society.

electronic structure can form in 2D distorted silicene layers (**Figure 11**a). Similar to graphene multilayers, silicene was also modified to produce moiré patterns by using an interlayer twisting angle of ≈21.8°. The results show that a periodic potential capable of modulating the electronic dispersion at vHs for silicene moiré superlattices, was generated.[174] Li et al. grew multilayer silicene samples on Ag (111) by molecular beam epitaxy. The 2D structure produced was in agreement with theoretical $AB\bar{A}$ $\sqrt{3}\times\sqrt{3}$ unit cell model predictions as shown in Figure 11a,b. Apart from explicitly explaining the 2D structure, Li et al. also found long periodic patterns (1.7 nm) which they further intuitively explored as moiré patterns. Interestingly, these long periods were then used to estimate the twisting angle as being 21.8° via the moiré equation

$$D = a/\left[2\sin\left(\frac{\theta}{2}\right)\right] \tag{7}$$

where a is the lattice length for silicene. This allows estimation of the miss-orientation angle "ϕ" between the $\sqrt{3}\times\sqrt{3}$ silicene lattice and the moiré superlattice, which in this case was estimated to be 19.1° and was confirmed by experiments.[174]

After structural elucidations with the help of DFT ab initio methods in combination with STM analysis, the electronic structure was carefully explored. The theoretical and experimental DOS observation also clearly shows the characteristics of the periodic moiré pattern in real space in the form of the occurrence of a hexagonal potential. Such a periodic potential pattern is inverted for energies higher than the Fermi level. Apart from Dirac points at –0.1 V (as shown in Figure 11). The STS scans across the moiré patterns also show discontinuities attributable to flat bands[175] that are consistent with both $\sqrt{3}\times\sqrt{3}$ silicene and a moiré superlattice. In contrast, dissimilarly, the moiré patterns of twisted silicene show distinct vHs at –1.2 and +0.75 V as can be seen in Figure 11f. The misalignment could have been caused by bending of the tipinduced band during scanning.[176] Overall, the twisted superlattice experiences rotation of the Brillouin zone by the same twisting angle. Owing to interlayer electron hopping, the overlapping Dirac cones generate two saddle points that are symmetric with respect to the Dirac point as also illustrated in Figure 11e. However, it was inferred from the angle-resolved photoemission spectroscopy (ARPES) measured Fermi velocity that interlayer coupling in silicene is much stronger, which enables vHs to be produced at larger angles such as 21.8°, as shown in Figure 11c,f. In comparison, this behavior disappears because the interlayer coupling in a graphene moiré superlattice breaks down for twisted angles exceeding 15°.[151] In a more recent study by Zhi et al., the moiré superlattice has been shown to produce moiré patterns in multilayer silicene. A low buckled electronic Kagomé lattice was induced under moiré interferences. Lattice impose quantum interferences formed unique 1D edge states localized at higher energies for such a 2D systems.[177]

In summary, silicene sp^2–sp^3 mixed hybridization states lead to enhanced robust interlayer interaction in multilayer silicene and this interaction is much stronger compared to that in multilayer graphene. Compared to the graphene moiré superlattice, silicene is therefore advantageous in that it allows interlayer hopping for even larger twisting angles, which is unachievable for graphene. This broadens the scope for engineering the electronic properties of multilayer moiré superlattice structures.

© 2020 WILEY-VCH Verlag GmbH & Co. KGaA, Weinheim

4.2. Phosphorene

2D black phosphorus (BP) has emerged as a dynamic electronic material because of its versatile electronic properties.[178] Exotic features, such as a tunable direct band,[179] high carrier mobility,[180] anisotropic Landau levels,[181,182] and interesting anomalous magneto-optical transport properties have already allowed its full potential to be unlocked in the science of advanced materials.[183–185] Modulation of the electronic structure of the moiré periodic potential has stimulated the exploration of modulation of the twist angle in 2D materials beyond graphene. Struck by current development, BP has also been fabricated and simulated for a range of twist angles to unlock the moiré bilayer superlattice, which is a new electronic phenomenon.[186–190] The stacking arrangements are shown to directly induce direct bandgaps ranging from 0.78 to 1.04 eV, which could be further developed provided the heterostructure with MoS_2 is determined to be an efficient effective solar-cell material with type-II heterojunction alignment.[191] Here, we review the potential contribution of phosphorene, with its anisotropic rectangular lattice, toward developing moiré physics.

Early first-principle studies of twisted bilayers showed that a large achievable twist angle between bilayers, such as 90°, imparts the ability to tune the anisotropy of the electronic structure and optical transitions by using simple gating methods manageable at the laboratory scale. A laboratory-accessible gate voltage can induce a hole effective mass that is 30 times larger along one of the axes compared to the other Cartesians, and two of the Cartesians can be inverted by flipping the sign of the gated voltage.[189] This was a significant improvement, adding to the available tunable degrees of freedom in black phosphorus with a twisted bilayer. However, thousands of atoms are required to model the moiré superlattice for very small twist angles and this superlattice has therefore become impossible to study within the framework of general Khon–Sham DFT.[187] Kang et al. overcame this problem by integrating LAMMPS[192] for structural relaxation and by analyzing the force fields of the mechanical properties. For the electronic and transport properties they used RESCU,[193] a MATLAB-based Kohn–Sham density functional theory (KS-DFT) solver. which uses the Chebyshev filtering technique., It basically exploits the fact that only a subspace spanning the occupied Kohn–Sham states is required, and solving accurately the KS equation using eigensolvers can generally be avoided.[194] This allowed them to compute the important physical parameters, which are listed in **Table 1**. Significant anisotropy was observed for the computed mobilities and this increases the degrees of freedom influencing the electronic structure of BP bilayer structures.

Recent experimental evidence shows that, for large twisting angles as observed by Fang et al., the interlayer interactions extend beyond vdW interactions and start to develop weak interlayer covalent bonding features.[189] These interactions clearly support the stronger interlayer coupling interactions in such a 2D twisted bilayer superlattice. The fact became evident from the abnormal blueshifts exhibited by their A_g^1 and A_g^2 Raman peaks and the correspondingly unique optical reflections attained in these samples, as shown in **Figure 12**. The use of DFT calculations also clearly suggested that the interlayer interactions were significantly stronger than simple interlayer coupling, such as in the twisted bilayer BP samples that were prepared.

A new study by Zhao et al., which surfaced very recently, shows deeper understanding toward this weak interlayer covalent bonding feature arising in twisted BP flakes, which they carefully prepared with twist angles in the range 2°–19°.[190] Similarly, a very recent DFT study of Liu et al. illustrates how the electronic properties can be tuned via interlayer twist dependent coupling effects of BP bilayers, as shown in **Figure 13**.[237] The interlayer cohesive energy varies in periodic interval of about 36⁰ for $E_{coh\ vs\ \theta}$ (Figure 13a). This periodicity is a direct influence of the coupling strength (α) of the two lone pairs orbital overlaps on the adjacent layers as illustrated in Figure 13a. Similar coupling was evident in work by Zhao et al.[190] The variation of band gap is shown as a function of twist angles in Figure 13c. Stronger interlayer interactions changes the intralayer and interlayer electron distributions and leads to anisotropic electronic[237] and vibrational properties.[190] Overall, the physical characteristics observed for large-angle twist moiré superlattices of BP differed from those of graphene because electronic structure modulation was achieved even for significantly larger twisting angles, as was observed in the case of silicene (discussed in Section 4.1).

The tremendous progress in fabricating and characterizing 2D vdW heterojunction materials is discussed in Section 2. The local potential induced by the moiré pattern and consequent wave-function localizations and the concomitant drastic reduction in the carrier mobility (as in BP) should be experimentally

Table 1. Structural information of all small twist angle moiré superlattice modeled for BP by Kang et al.[187] The untwisted BP is formed by expanding the primitive cell of BP (AA stacking) with a factor of p and n along the x and y directions, respectively. Alongside crystal information, additional computed effective masses and motilities by means of deformation potential method are also listed. From the listed data, it can be roughly concluded that the moiré pattern wavelength roughly varies inversely to twisting angles, and electronic mobility has much more pronounced effects of twisting angles.

Twist angle [θ]	0°	1.8°	2.2°	2.7°	3.6°	5.4°
Number of atoms	8	8068	5604	3588	2020	900
$n \times p$	1×1	24×42	20×35	16×28	12×21	8×14
Supercell size [Å]	3.31×4.38	140.70×106.35	117.25×88.63	93.90×70.98	70.35×53.17	47.00×35.35
m_e*	0.13	0.84	0.45	0.29	0.20	0.17
m_h*	0.12	0.16	0.16	0.16	0.16	0.16
μ_e	2.56	0.13	0.41	1.14	2.25	5.06
μ_h	4.46	4.55	4.48	4.79	5.06	4.75

© 2020 WILEY-VCH Verlag GmbH & Co. KGaA, Weinheim

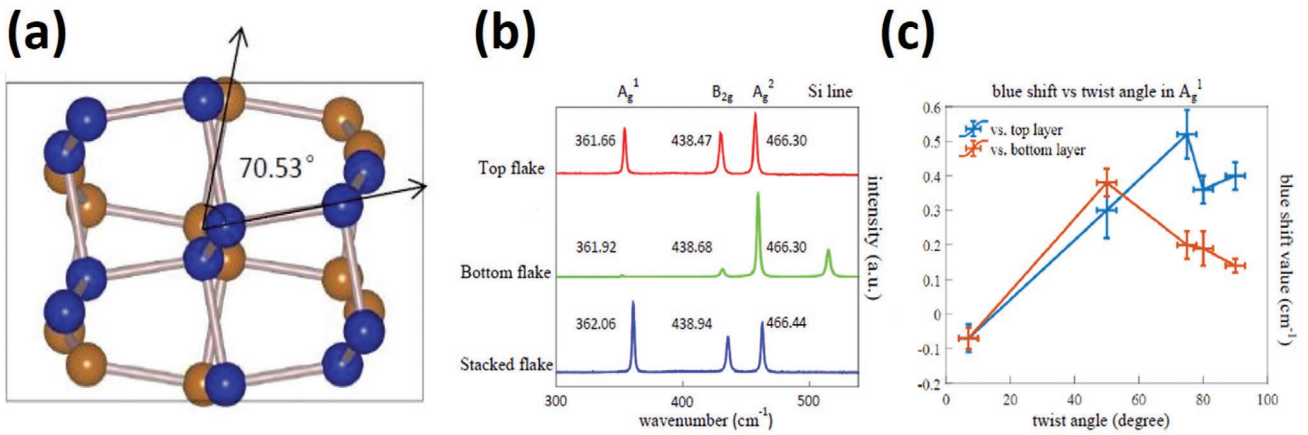

Figure 12. a,b) The crystal structure of 70.53° twisted bilayer BP a), along with an illustration of three high-frequency Raman active phonon modes in BP b). The A_g^1 mode has a vibration direction perpendicular to the 2D BP plane, so interlayer coupling exerts more influence on it. c) Plot of the blueshift value versus twist angle in A_g^1, B_{2g}, and A_g^2. Values of the top layer and bottom layer are plotted separately. Reproduced with permission.[188] Copyright 2019, ACS.

verifiable by STM/STS methods, and could provide an interesting strategy for designing nanoelectronic devices.

4.3. Van der Waals Heterostructures

The first moiré superlattice that was critically observed for incommensurate heterostructures was that of graphene/BN.[102] This heterostructural superlattice provided unprecedented experimental access to the fractal spectrum and led to the first ever study of Hofstadter's butterfly and the fractal quantum Hall effect in the moiré´ superlattice of vdW heterostructures of graphene and BN.[154,195] Apart from this study, the last decade has not seen many investigations pertaining to such a moiré pattern generated for incommensurate heterostructures.

However, in 2019, Zhang et al. fabricated a range of structures with a twist angle between monolayer BP and monolayer MoS_2 with the intention to study the band modulation effects using ab initio (first principle) calculations. The bandgap was significantly altered with no notable trend in the range 0.51, 0.72, 0.48, and 0.85 eV for periodic supercells molded by twist angles of 0°, 36.10°, 90°, and 125.44°, respectively. Generally, the positions and orbital contributions of conduction band minima (CBM) and valance band maxima (VBM) in BP/MoS_2 heterojunctions are altered as the two layers twist relative to each other, while the major orbital contributions, i.e., the d_{z^2} states of the Mo atoms and p_z states of the P atoms, remain unchanged. However, application of an electric field to these twisted BP/MoS_2 heterostructures results in bandgap transitions from indirect-to-direct and direct-to-indirect transformations.[196] This opens up the opportunity for band modulations and for optimizing the electronic structure for photovoltaic and relevant applications.

STM has become an essential tool to explore the moiré patterns in twisted flatland materials. One such very recent study was carried out by Ster et al., who explored 2D allotropes of bismuth and antimony grown on highly ordered pyrolytic graphite and MoS_2. They modeled the structures by fitting their experimental observations using a simple superposition model. This allowed them to explain the moiré pattern formed by mixed stacking sequences without relying on commensuration of the layered structures.[197] Their study is a first of its kind for interpreting the moiré patterns of any pair of 2D layered stacks. However, this also shows the vast opportunities that remain undeveloped owing to the dearth of explorations and the unavailability of comprehensive knowledge of this class of moiré patterns.

This unique rotational degree of freedom could provide unmatchable control over flatland materials by tuning their atomic structures for the moiré potential; consequently, this could result in the discovery of electronic structures for advanced electronic applications. A particular class of materials that has seen significant advancement because of their

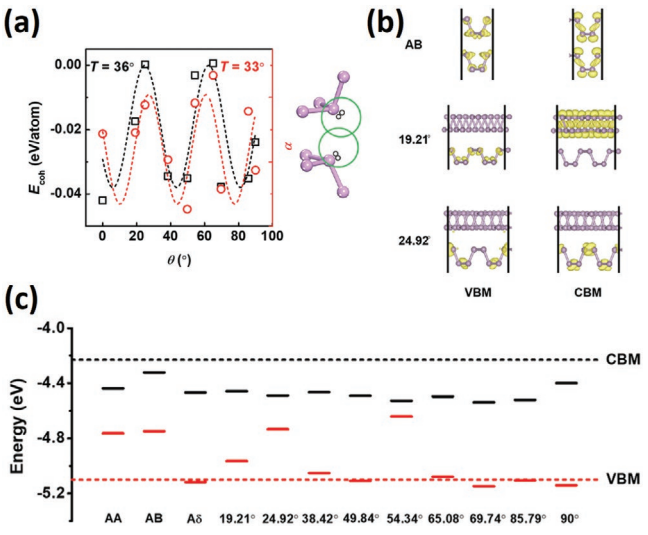

Figure 13. a) The Cohesive energy (E_{coh}) and coupling strength (α) of lone pairs as a function of twist angle (θ) with approximate oscillation periods of 36° and 33°, respectively. b) Partial charge density of CBM and VBM and electrostatic potential along z direction for AB, and θ = 19.211 and 24.921, respectively. c) Band positions for bilayer BP with various twist angles. The dashed black and red lines are the CBM and VBM of monolayer BP. The vacuum level is set to zero. Reproduced with permission.[237] Royal Society of Chemistry.

© 2020 WILEY-VCH Verlag GmbH & Co. KGaA, Weinheim

heterostructural moiré patterns are TMDCs, which are reviewed separately below.

5. Moiré Excitons

The emerging physics of moiré patterns in twisted bilayer graphene has already led to exotic unprecedented electronic structural phenomena, such as the observation of vHs,[5] band flattening,[156] the fractal quantum Hall effect,[88,195] tunable Mott insulators,[83,198] and unconventional superconductivity.[84] Undoubtedly, after graphene, one of the most popular 2D materials is MoS_2, a TMDC.[199–201] We thus focus on discussing the way in which developments in twisted graphene have inspired the initial footsteps to investigate twisted bilayer TMDCs. This has proven to provide altogether new freedom of control over optically important moiré excitons. Strong intralayer covalent bonding makes it possible to exfoliate these materials, similar to graphene, but it also conveys unique semiconducting properties, in sharp contrast to graphene. This semiconducting nature also distinctively renders it optically active, thereby giving it a broader role in electronic and optoelectronic applications.[200–202]

Among the growing population of flatland materials, TDMCs are highly sensitive to crystal structure symmetry and interlayer coupling.[203–206] This also makes them highly susceptible to stacking sequences, considering that we are focusing on periodic moiré patterns generated as a result of a slight shift in otherwise perfectly aligned monolayer stacks. Here for TMDCs, on the basis of the nature of the monolayers that form a moiré superlattice, we divide moiré superlattices into those that form either homobilayer or heterobilayer moiré patterns. Further, a heterobilayer moiré superlattice can readily be generated as a result of lattice mismatch or further can be amended via interlayer twists similar to the moiré superlattice of graphene/BN heterobilayers, as discussed in Section 2.1.

5.1. Homobilayer Moiré Superlattice

Parallel to the moiré superlattice in graphene, scientific intuition guided by theoretical predictions has paved the way toward discovering notable effects of optical excitations in TMDCs,[86,90,91,207] which are influenced directly by the moiré potential in 2D valley semiconductors.[207–209] Naik and Jain performed first-principal calculations on MoS_2 and were able to discover band flattening analogous to that of graphene at the valence band edge of the homobilayer moiré superlattice for twist angles of 56.5° and 3.5°.[210] The observed flattening of the valence band was accompanied by electrons that are spatially localized entirely at the AB stacked regions for a relaxed atomic moiré superlattice. This was predicted to directly influence the dynamics of excitons.[210]

STM analysis supported by electronic structure calculations also proved that the bilayer separation varied as a function of twist. As the sulfur atoms at the interface experience repulsions, the indirect optical transition energies subsequently undergo pronounced shifts, as shown in **Figure 14**.[211,212] Ye et al. directly analyzed the influence of the twist angle of the indirect bandgaps of MoS_2. They used a dry transfer process to carefully stack CVD-grown flakes of MoS_2 to obtain different twist angles. This involved dividing the MoS_2 flakes over the SiO/Si substrate into upper and lower sections. Later, each section was carefully transferred to polymethyl methacrylate (PMMA) to enable the SiO/Si substrate to be etched. The PMMA-supported section of the MoS_2 flake can be covered with a glass slide coated with polydimethylsiloxane. The next step was to realign the two parted sections on top of each other to form a stack with a variety of twist angles.[213]

Analysis of the electronic structure by angle-resolved photoemission spectroscopy showed band variations between the flakes twisted at angles of 0°, 13.5°, 26.5°, 39°, 47.5°, and 60°. The change in indirect band edges for the VBM and CBM observed between the Γ and K points, respectively, for dispersion along high symmetry points is discernible with different twists as shown in Figure 14. It can be concluded, from work carried out by Naik et al. and confirmed by photoluminescence measurements,[211,213–215] that variation of the bandgap is mainly attributable to the energy change of the VBM at Γ, which shows that the bandgap depends more strongly on the interlayer distance, which directly determines the coupling strengths. However, the interlayer twists indirectly allow the interlayer distances to be dictated and weakly depend on the change in the energy of the VBM, which allows new freedom for electronic structure modulations.

These findings have a direct impact on future developments by providing physical insight into the optical and electronic properties of the moiré superlattice of TMDCs. The bandgap, electron transport, and spin/valley properties can be controlled by tuning the interlayer coupling, because the ability to control the interlayer coupling is important for the development of TMDC-based devices.

5.2. Heterobilayer Moiré Superlattice

Facile exfoliation is a significant benefit of a compact strong covalent monolayer framework with weak interlayer attractions. This also allows the TMDC layer to be readily interchanged to form artificial heterobilayer structures currently more commonly known as heterostructures. The large family of TMDCs includes layered materials with various types of electronic structures, from semiconducting to semimetallic to metallic in nature. These heterostructures offer the possibility to engineer new materials by modifying the interlayer interactions. These modifications have become achievable by using careful transfer[216–218] or CVD growth methods.[219] Considering the entire collection of known TMDC layered crystals, one feature that stands out is their direct-band semiconductor electronic structure, which allows these materials to interact with light.[220–222] Heterobilayers stacked on top of each other are known to produce type-II band alignments,[223,224] which actually constitutes CMB and VBM localization into different layers. This naturally results in photoexcited electrons and holes being produced in different layers.[225–229] However, strong Coulomb interaction among these interlayer pairs keep them bound; hence, they are more generally referred to as interlayer excitons, as illustrated clearly in **Figure 15**.[230,231]

The fabrication of heterojunctions does not only give rise to modifications of the electronic structure. Generally, the two layers to be stacked upon each other are most likely to have

© 2020 WILEY-VCH Verlag GmbH & Co. KGaA, Weinheim

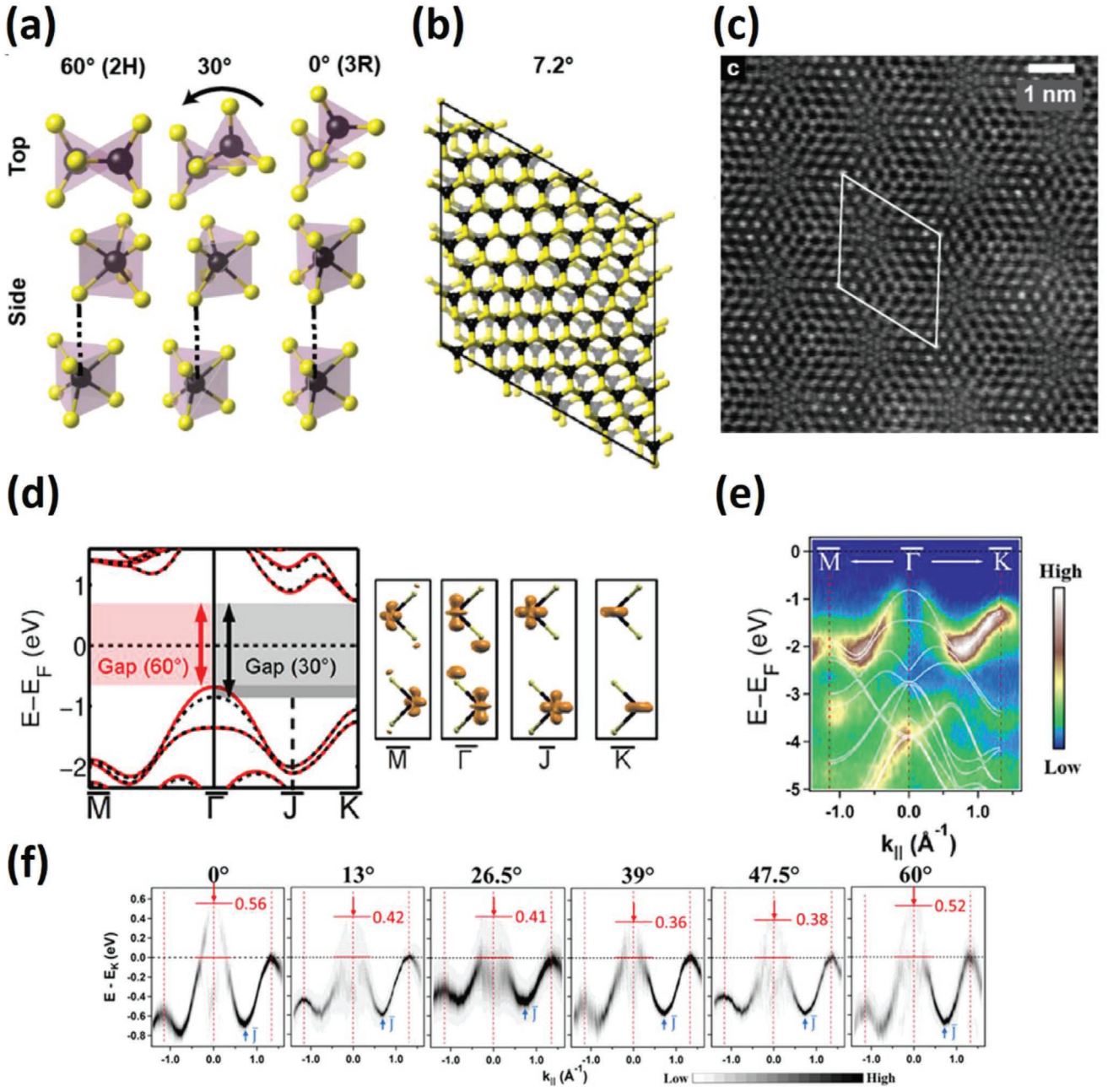

Figure 14. a) Homobilayer crystal structures alignment showing bilayer MoS_2 with twist angles of 60° (2H phase), 30°, and 0° (3R phase). b,c) MoS_2 moiré superlattice unit cell for a bilayer structure with a twist angle of 7.2° b) along with high-resolution ADF-STM image of an experimentally fabricated bilayer with a twist angle of 8.5° and a moiré quasiperiodicity of 2.5 nm c). a–c) Reproduced with permission.[211] Copyright 2014, American Chemical Society. d) DFT calculated electronic band dispersions for 60° and 30° twisted MoS_2 bilayers overlays shown by red and black dash bands along with band decomposed charge densities for M–Γ–J–K high-symmetry points along the BZ path. d–f) ARPES measured band dispersion for M–Γ– K overland with white lines from DFT calculation along with the bottom section showing ARPES measurements for samples with various twist angles (i.e., 0°, 13.5°, 26.5°, 39°, 47.5°, and 60°) prepared by a dry-transfer method. d–f) Reproduced with permission.[212] Copyright 2016, American Chemical Society.

different lattice parameters. This situation is conducive for the creation of incommensurate monolayer periodic moiré patterns for a heterostructural lattice. These moiré patterns can be amended by adjusting the interlayer twist angles of these heterobilayer moiré superlattices. In these moiré superlattices, the metal heteroatoms (i.e., Mo and W) of neighboring layers appear on top of each other only for periodic moiré wavelengths. Atoms stacked in different configurations are known as registries, which also cause the valence and conduction bands to have different energies, which is STM verifiable, as shown in Figure 15a for the MoS_2/WSe_2 heterobilayer moiré superlattice.[219] These conditions lead to the formation of periodically changing bands, which can trap electrons at the moiré potential, if the variation in the band energies is sufficiently large. The periodic moiré

© 2020 WILEY-VCH Verlag GmbH & Co. KGaA, Weinheim

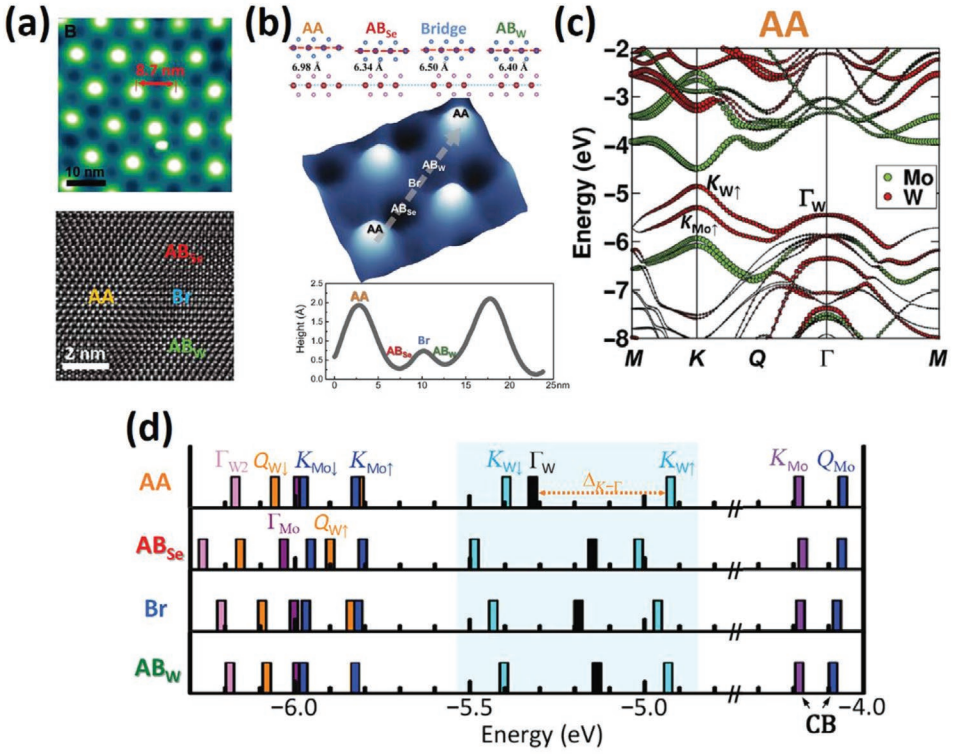

Figure 15. a,b) STM image of the moiré pattern a), and STM image for atomic resolution, zoomed-in b). The description for four different periodic registries along moiré superlattice vector and their interlayer distances from rotationally aligned models are denoted as AA, Br, AB_W, and AB_{Se}. c,d) The weighted electronic band dispersion showing the direct type-II band alignment at the K point of the BZ along with theoretical posterior strain corrected shifting of critical points as highlighted in band structure showing direct change under different denoted registries. a–d) Reproduced with permission.[219] Copyright 2019, The Authors, published by American Association for the Advancement of Science.

obtained in this way can be controlled and tuned by engineering the interlayer twist. Consequently, the electronic properties can be controlled by exploiting an entirely new degree of freedom for an optically important collection of flatland materials.[86]

Figure 15b shows the four periodic configurational points of the MoS_2/WSe_2 moiré superlattice and these are denoted as AA, AB_{Se}, Br, and AB_W for convenience, depending on which atoms from opposite interlayers are facing each other (Br denotes atoms facing bridges of the opposite layer). Zhang et al. calculated the electronic structure for all four of these registry points for the rotationally aligned structure. Representative models show that direct band type-II alignments are preserved with the CBM and VBM located in the MoS_2 and WSe_2 monolayers, respectively (Figure 15c). However, for the four point representative models the interlayer distances were calculated to decrease in the order AA > Br > AB_W> AB_{Se}. Along with their calculations, Zhang et al. also presented a careful analysis of the band variations using STM/STS.[219] This study showed that the registry between vdW layers dictates the behavior of interlayer electronic coupling, control over which could be expected to allow novel 2D electronic systems based on vdW heterostructures. Later, Yu et al. showed that the vdW heterostructures of 2D semiconductors are naturally endowed with an ordered nanoscale landscape, i.e., a moiré pattern, which laterally modulates electronic and topographic structures.[89] They were able to realize a wide-range-tunable wavelength of long-lived wavelength excitons, whereas among other moiré effects, these excitons could be made to flip the spin optical selection rule of the periodic emitter arrays by electric field.

Four recent papers reported investigations of the interaction of light with twisted heterobilayer moiré superlattices of TMDCs. The investigation revealed larger variations in energies for changing registries occurring at the moiré wavelength of heterobilayer TMDC structures. Two of these investigations focused on the $MoSe_2/WSe_2$ heterobilayer moiré superlattice. Tran et al. studied samples of the $MoSe_2/WSe_2$ moiré superlattice prepared with a small rotational misalignment. The novelty of their work was that it provided experimental insight into the optical properties. They were able to locate the peaks of interlayer excitons on the emission spectra, and determined the extent to which the energy separation between peaks and polarization of the emission depended on the twist angle of the moiré superlattice structure.[90] In their original report, they hinted toward the need to conduct an experiment to resolve individual interlayer excitons confined within a supercell. The experiment would involve the implementation of either a near-field optical probe or combined STM and optical spectroscopy studies, and would help to further establish the influence of the moiré potential. Seyler et al. studied individual interlayer excitons trapped by the moiré potential for the same system, i.e., a $MoSe_2/WSe_2$ heterobilayer moiré superlattice.[91] Their observations include highly polarized emission spectral lines, which they further split into multiple peaks by applying a magnetic field. The emission line spectra deliver a fingerprint of the

© 2020 WILEY-VCH Verlag GmbH & Co. KGaA, Weinheim

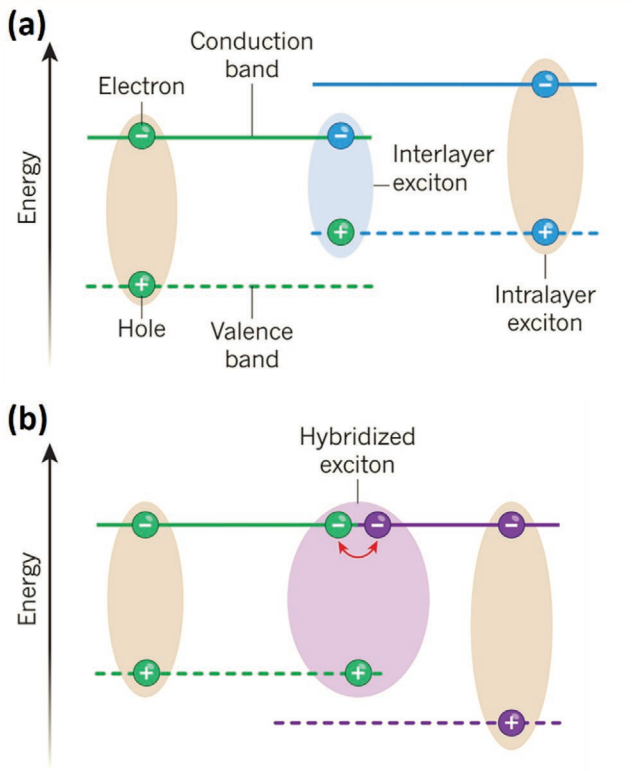

Figure 16. Schematic illustrations of excitonic formation under heterojunctions formed by TMDCs. a) Interlayer excitones produced under CBM and VBM localizations on different layers, whereas Alexeev et al.[232] observed that b) conduction band can disperse over both heterobilayers to give hybrid excitones. Reproduced with permission.[235] Copyright 2019, Springer Nature.

magnetic moment and the minima or maxima of each valley of the electronic band dispersion of the pairs (i.e., electron–hole pairs) that formed a specific exciton. Apart from this, in work carried out by Seyler et al., many separate peaks were detected within the laser excitation spot, which points toward inhomogeneity in the moiré superlattice potential, thereby resulting in nondegeneracy traps. More precise fabrication techniques with accurate scanning techniques are expected to deliver improved results. Another very recent study, which was carried out by Jin et al., revolved around light adsorption as a result of the moiré potential. This phenomenon was examined by fabricating a slightly different system consisting of WSe_2/WS_2 for experimental investigations.[232,234–236] Comparison of the conventional WSe_2-A exciton resonance on the absorption spectra was sufficient to distinguish multiple emergent peaks from moiré excitons as they were also found to be distinctly gate dependent. Jin et al. fitted a theoretical model and showed that a stronger moiré potential becomes the foundation for the generation of multiple flat exciton minibands. The last of the four papers presents an interesting and entirely new concept of hybrid excitons. Alexeev et al. discovered that intralayer excitons can proceed via a mix-up (hybridized) with interlayer excitons.[233] Their study of $MoSe_2/WS_2$ revealed that the conduction band is delocalized over both layers of the moiré heterojunction. This feature was also found to amplify the influence of the moiré potential on the optical features of these heterojunctions. The optical features that were explored in these four recent papers are summarized in **Figure 16**. However, these studies are expected to be only the first small footsteps toward the complete understanding and control over individual moiré potentials. Thus, in-depth knowledge of the size and depth of these potentials is expected to lead to the discovery of single exciton traps. This offers the potential for obtaining tunable periodic light emitters in the fascinating world of twisted flatland materials.

6. Summary and Outlook

In summary, the craft of producing emerging flatland materials with a moiré superlattice has led to exceptional breakthroughs in recent years. These visually beautiful patterns that are generated as a result of the rotational misalignment of commensurate layers or by mismatching lattices of incommensurate layered structures directly influence the electronic structures of 2D materials. Interlayer twist provides entirely new opportunities to tailor the electronic properties of 2D van der Waals materials. However, it remains difficult to control these twist angles when fabricating new structures. Recent encouraging developments have made it possible to more accurately control and stack the layers by using a variety of fabrication methods, such as epitaxial growth, CVD, monolayer folding, pick-up, and transfer methods, as well as the fabrication of devices with dynamically rotatable monolayers. The demonstration of fabricated moiré superlattice structures in recent years are foreseen to lead to the development of state-of-the-art twistronics with emergent material phases endowed with exotic properties, such as superconductivity and magnetism, which may be controlled by varying the rotation.

Recent advances in STM/STS has enabled investigations to be carried out that provide new insights into electronic structure modulations for very small so-called magic-angle band flattening in twisted bilayer graphene layers. These flat bands happen to oscillate to generate two intrinsically different phases, one strongly correlated insulating (CI) and the other superconducting, for different carrier concentrations. Magic-angle twisted bilayer graphene is already providing us with a new understanding of superconductivity in a strongly correlated system. In terms of the design of new superconductors with a record high critical temperature, "T_c," twisted bilayer graphene provides a clean and highly tunable platform to serve as testing ground. Apart from STM/STS analysis, valuable insights could be obtained by using higher resolution and more sophisticated techniques such as ARPES. However, this is simply a new beginning filled with surprises along the twisted bilayer graphene track. In this regard, materials such as silicene have already broadened the scope by exhibiting interlayer hopping, even for larger twist angles, which is unachievable for the graphene moiré superlattice.

In parallel to the enhanced understanding of the moiré superlattice is the establishment of a semiconductor class of flatland materials. In particular, the twist angle of phosphorene was shown to directly influence the localization of the electronic wave function in free space and this is accompanied by concomitant drastic reduction of the carrier mobility. The Raman peaks of twisted stacked systems are indicative of stronger interlayer coupling. The other development that took place is

© 2020 WILEY-VCH Verlag GmbH & Co. KGaA, Weinheim

that evidence of the existence of localized moiré excitons was found within the moiré superlattice of heterobilayer TMDCs. The discovered optical phenomenon could lead to highly tunable quantum arrays under the influence of periodically modulated moiré potential. The strong interlayer coupling in heterostructures can induce distinct concentrated regions of excitons. This produces additional moiré excitons that are specially trapped in well-separated moiré potential wells to consequently form a quantum array in the extended moiré superlattice. Most importantly, the condensed exciton bandwidth also renders this artificially produced exciton superlattice a promising platform to realize unprecedented exotics, such as a topological exciton insulator or a strongly correlated exciton Hubbard model. Apart from type-II alignments, resonant interlayer hybridization in the $MoSe_2/WS_2$ structure is exciting as it happens to produce hybridized exciton states that inherently show the spectral properties of both intralayer and interlayer excitons. For such a material, the twist-angle-controllable resonant effects could establish a new approach for engineering carriers and the exciton band-structure by fabricating flatland materials with a moiré superlattice.

Acknowledgements

This work was supported by the State Key Research Development Program of China (Grant No. 2019YFB2203503), National Natural Science Fund (Grant Nos. 61875138, 61435010, and 61961136001), and Science and Technology Innovation Commission of Shenzhen (Nos. JCYJ20190808112401659, KQTD2015032416270385, and JCYJ20170811093453105). The authors also acknowledge support from Clean Energy Institute of Shenzhen and the Instrumental Analysis Center of Shenzhen University (Xili Campus).

Conflict of Interest

The authors declare no conflict of interest.

Keywords

2D materials, graphene, interlayer twists, moiré patterns, superlattices

Received: January 30, 2020
Revised: April 9, 2020
Published online: July 16, 2020

[1] A. K. Geim, I. V. Grigorieva, *Nature* **2013**, *499*, 419.
[2] K. S. Novoselov, A. Mishchenko, A. Carvalho, A. H. C. Neto, *Science* **2016**, *353*, aac9439.
[3] K. S. Novoselov, A. K. Geim, S. V. Morozov, D. Jiang, Y. Zhang, S. V. Dubonos, I. V. Grigorieva, A. A. Firsov, *Science* **2004**, *306*, 666.
[4] K. S. Novoselov, D. Jiang, F. Schedin, T. J. Booth, V. V. Khotkevich, S. V. Morozov, A. K. Geim, *Proc. Natl. Acad. Sci. USA* **2005**, *102*, 10451.
[5] G. Li, A. Luican, J. L. Dos Santos, A. C. Neto, A. Reina, J. Kong, E. J. N. P. Andrei, *Nat. Phys.* **2010**, *6*, 109.
[6] K. Liu, L. Zhang, T. Cao, C. Jin, D. Qiu, Q. Zhou, A. Zettl, P. Yang, S. G. Louie, F. Wang, *Nat. Commun.* **2014**, *5*, 4966.
[7] T. Jiang, H. Liu, D. Huang, S. Zhang, Y. Li, X. Gong, Y. R. Shen, W. T. Liu, S. Wu, *Nat. Nanotechnol.* **2014**, *9*, 825.
[8] Y. Liu, N. O. Weiss, X. Duan, H.-C. Cheng, Y. Huang, X. Duan, *Nat. Rev. Mater.* **2016**, *1*, 16042.
[9] Z. Shi, X. Wang, Y. Sun, Y. Li, L. Zhang, *Semicond. Sci. Technol.* **2018**, *33*, 093001.
[10] Z. Guo, S. Chen, Z. Wang, Z. Yang, F. Liu, Y. Xu, J. Wang, Y. Yi, H. Zhang, L. Liao, *Adv. Mater.* **2017**, *29*, 1703811.
[11] S. C. Dhanabalan, J. S. Ponraj, Z. Guo, S. Li, Q. Bao, H. Zhang, *Adv. Sci.* **2017**, *4*, 1600305.
[12] L. Zhao, D. Tang, H. Zhang, X. Wu, N. Xiang, *Opt. Express* **2008**, *16*, 9528.
[13] W. Liao, Y. Huang, H. Wang, H. Zhang, *Appl. Mater. Today* **2019**, *16*, 435.
[14] H. Zhang, D. Y. Tang, L. M. Zhao, R. J. Knize, *Opt. Express* **2010**, *18*, 4428.
[15] L. Kong, Z. Qin, G. Xie, Z. Guo, H. Zhang, P. Yuan, L. Qian, *Laser Phys. Lett.* **2016**, *13*, 045801.
[16] H. Zhang, D. Tang, L. Zhao, Q. Bao, K. P. Loh, **2010**, *283*, 3334.
[17] Y. Zhang, B. Lin, S. C. Tjin, H. Zhang, G. Wang, P. Shum, X. Zhang, *Opt. Express* **2010**, *18*, 26345.
[18] M. Liu, N. Zhao, H. Liu, X.-W. Zheng, A.-P. Luo, Z.-C. Luo, W.-C. Xu, C.-J. Zhao, H. Zhang, S.-C. Wen, *IEEE Photonics Technol. Lett.* **2014**, *26*, 983.
[19] J. Li, H. Luo, B. Zhai, R. Lu, Z. Guo, H. Zhang, Y. Liu, *Sci. Rep.* **2016**, *6*, 30361.
[20] J. Lu, K. Zhang, X. F. Liu, H. Zhang, T. C. Sum, A. H. C. Neto, K. P. Loh, *Nat. Commun.* **2013**, *4*, 2681.
[21] L. Zhao, D. Tang, X. Wu, H. Zhang, *Opt. Lett.* **2010**, *35*, 2756.
[22] Y. Chen, C. Zhao, S. Chen, J. Du, P. Tang, G. Jiang, H. Zhang, S. Wen, D. Tang, *IEEE J. Sel. Top. Quantum Electron.* **2014**, *20*, 315.
[23] Y. Chen, M. Wu, P. Tang, S. Chen, J. Du, G. Jiang, Y. Li, C. Zhao, H. Zhang, S. Wen, *Laser Phys. Lett.* **2014**, *11*, 055101.
[24] H. Zhang, D. Y. Tang, L. M. Zhao, H. Y. Tam, *Opt. Lett.* **2008**, *33*, 2317.
[25] H. Mu, Z. Wang, J. Yuan, S. Xiao, C. Chen, Y. Chen, Y. Chen, J. Song, Y. Wang, Y. Xue, *ACS Photonics* **2015**, *2*, 832.
[26] X. Ren, Z. Li, Z. Huang, D. Sang, H. Qiao, X. Qi, J. Li, J. Zhong, H. Zhang, *Adv. Funct. Mater.* **2017**, *27*, 1606834.
[27] X. Jiang, S. Liu, W. Liang, S. Luo, Z. He, Y. Ge, H. Wang, R. Cao, F. Zhang, Q. Wen, J. Li, Q. Bao, D. Fan, H. Zhang, *Laser Photonics Rev.* **2018**, *12*, 1700229.
[28] H. Zhang, D. Y. Tang, L. M. Zhao, X. Wu, *Phys. Rev. B* **2009**, *80*, 052302.
[29] J. Liu, Y. Chen, P. Tang, C. Xu, C. Zhao, H. Zhang, S. Wen, *Opt. Express* **2015**, *23*, 6418.
[30] P. Yan, R. Lin, H. Chen, H. Zhang, A. Liu, H. Yang, S. Ruan, *IEEE Photonics Technol. Lett.* **2015**, *27*, 951.
[31] L. Lu, Z. Liang, L. Wu, Y. Chen, Y. Song, S. C. Dhanabalan, J. S. Ponraj, B. Dong, Y. Xiang, F. Xing, D. Fan, H. Zhang, *Laser Photonics Rev.* **2018**, *12*, 1700221.
[32] B. Wang, H. Yu, H. Zhang, C. Zhao, S. Wen, H. Zhang, J. Wang, *IEEE Photonics J.* **2014**, *6*, 1501007.
[33] L. Lu, X. Tang, R. Cao, L. Wu, Z. Li, G. Jing, B. Dong, S. Lu, Y. Li, Y. Xiang, J. Li, D. Fan, H. Zhang, *Adv. Opt. Mater.* **2017**, *5*, 1700301.
[34] Y. Jiang, L. Miao, G. Jiang, Y. Chen, X. Qi, X.-f. Jiang, H. Zhang, S. Wen, *Sci. Rep.* **2015**, *5*, 16372.
[35] L. M. Zhao, D. Y. Tang, H. Zhang, T. H. Cheng, H. Y. Tam, C. Lu, *Opt. Lett.* **2007**, *32*, 1806.
[36] L. M. Zhao, D. Y. Tang, H. Zhang, X. Wu, *Opt. Express* **2008**, *16*, 10053.
[37] Q. Wang, Y. Chen, L. Miao, G. Jiang, S. Chen, J. Liu, X. Fu, C. Zhao, H. Zhang, *Opt. Express* **2015**, *23*, 7681.
[38] Y. F. Song, H. Zhang, D. Y. Tang, D. Y. Shen, *Opt. Express* **2012**, *20*, 27283.

 © 2020 WILEY-VCH Verlag GmbH & Co. KGaA, Weinheim

[39] H. Zhang, D. Tang, L. Zhao, X. Wu, *Opt. Express* **2011**, *19*, 3525.
[40] M. Liu, Z.-R. Cai, S. Hu, A.-P. Luo, C.-J. Zhao, H. Zhang, W.-C. Xu, Z.-C. Luo, *Opt. Lett.* **2015**, *40*, 4767.
[41] Z. Guo, H. Zhang, S. Lu, Z. Wang, S. Tang, J. Shao, Z. Sun, H. Xie, H. Wang, X. F. Yu, *Adv. Funct. Mater.* **2015**, *25*, 6996.
[42] Y. Wang, F. Zhang, X. Tang, X. Chen, Y. Chen, W. Huang, Z. Liang, L. Wu, Y. Ge, Y. Song, J. Liu, D. Zhang, J. Li, H. Zhang, *Laser Photonics Rev.* **2018**, *12*, 1800016.
[43] Y. Xu, Z. Wang, Z. Guo, H. Huang, Q. Xiao, H. Zhang, X.-F. Yu, *Adv. Opt. Mater.* **2016**, *4*, 1223.
[44] Y. Xu, X.-F. Jiang, Y. Ge, Z. Guo, Z. Zeng, Q.-H. Xu, H. Zhang, X.-F. Yu, D. Fan, *J. Mater. Chem. C* **2017**, *5*, 3007.
[45] Z. Li, H. Qiao, Z. Guo, X. Ren, Z. Huang, X. Qi, S. C. Dhanabalan, J. S. Ponraj, D. Zhang, J. Li, J. Zhao, J. Zhong, H. Zhang, *Adv. Funct. Mater.* **2018**, *28*, 1705237.
[46] Y. Ge, Z. Zhu, Y. Xu, Y. Chen, S. Chen, Z. Liang, Y. Song, Y. Zou, H. Zeng, S. Xu, H. Zhang, D. Fan, *Adv. Opt. Mater.* **2018**, *6*, 1701166.
[47] Y. Song, Z. Liang, X. Jiang, Y. Chen, Z. Li, L. Lu, Y. Ge, K. Wang, J. Zheng, S. Lu, *2D Mater.* **2017**, *4*, 045010.
[48] Y. Song, Y. Chen, X. Jiang, W. Liang, K. Wang, Z. Liang, Y. Ge, F. Zhang, L. Wu, J. Zheng, J. Ji, H. Zhang, *Adv. Opt. Mater.* **2018**, *6*, 1701287.
[49] R. Cao, H. D. Wang, Z. N. Guo, D. K. Sang, L. Y. Zhang, Q. L. Xiao, Y. P. Zhang, D. Y. Fan, J. Q. Li, H. Zhang, *Adv. Opt. Mater.* **2019**, *7*, 1900020.
[50] Y. Ge, S. Chen, Y. Xu, Z. He, Z. Liang, Y. Chen, Y. Song, D. Fan, K. Zhang, H. Zhang, *J. Mater. Chem. C* **2017**, *5*, 6129.
[51] Q. Wu, S. Chen, Y. Wang, L. Wu, X. Jiang, F. Zhang, X. Jin, Q. Jiang, Z. Zheng, J. Li, *Adv. Mater. Technol.* **2019**, *4*, 1800532.
[52] S. Meng, T. Kong, W. Ma, H. Wang, H. Zhang, *Small* **2019**, *15*, 1902691.
[53] R. Wang, X. Jiang, S. Gao, J. Zhao, F. Zhang, W. Huang, T. Fan, W. Liang, Z. Li, H. Huang, *Adv. Mater. Interfaces* **2019**, *6*, 1900171.
[54] Y. Yin, R. Cao, J. Guo, C. Liu, J. Li, X. Feng, H. Wang, W. Du, A. Qadir, H. Zhang, *Laser Photonics Rev.* **2019**, *13*, 1900032.
[55] J. Zhao, J. Zhu, R. Cao, H. Wang, Z. Guo, D. K. Sang, J. Tang, D. Fan, J. Li, H. Zhang, *Nat. Commun.* **2019**, *10*, 1.<./bib>
[56] L. Britnell, R. V. Gorbachev, R. Jalil, B. D. Belle, F. Schedin, A. Mishchenko, T. Georgiou, M. I. Katsnelson, L. Eaves, S. V. Morozov, N. M. R. Peres, J. Leist, A. K. Geim, K. S. Novoselov, L. A. Ponomarenko, *Science* **2012**, *335*, 947.
[57] H. Yang, J. Heo, S. Park, H. J. Song, D. H. Seo, K. E. Byun, P. Kim, I. Yoo, H. J. Chung, K. Kim, *Science* **2012**, *336*, 1140.
[58] T. Georgiou, R. Jalil, B. D. Belle, L. Britnell, R. V. Gorbachev, S. V. Morozov, Y. J. Kim, A. Gholinia, S. J. Haigh, O. Makarovsky, L. Eaves, L. A. Ponomarenko, A. K. Geim, K. S. Novoselov, A. Mishchenko, *Nat. Nanotechnol.* **2013**, *8*, 100.
[59] L. Su, X. Fan, T. Yin, H. Wang, Y. Li, F. Liu, J. Li, H. Zhang, H. Xie, *Adv. Opt. Mater.* **2020**, *8*, 1900978.
[60] R. Wang, X. Li, Z. Wang, H. Zhang, *Nano Energy* **2017**, *34*, 131.
[61] D. K. Sang, H. Wang, Z. Guo, N. Xie, H. Zhang, *Adv. Funct. Mater.* **2019**, *29*, 1903419.
[62] Y. Li, R. Wang, Z. Guo, Z. Xiao, H. Wang, X. Luo, H. Zhang, *J. Mater. Chem. A* **2019**, *7*, 25227.
[63] Q. Jiang, L. Xu, N. Chen, H. Zhang, L. Dai, S. Wang, *Angew. Chem., Int. Ed.* **2016**, *55*, 13849.
[64] Y. Sun, F. Lei, S. Gao, B. Pan, J. Zhou, Y. Xie, *Angew. Chem., Int. Ed.* **2013**, *52*, 10569.
[65] W. Han, C. Zang, Z. Huang, H. Zhang, L. Ren, X. Qi, J. Zhong, *Int. J. Hydrogen Energy* **2014**, *39*, 19502.
[66] A. A. Ismail, D. W. Bahnemann, *Sol. Energy Mater. Sol. Cells* **2014**, *128*, 85.
[67] H. Liu, K. Hu, D. Yan, R. Chen, Y. Zou, H. Liu, S. Wang, *Adv. Mater.* **2018**, *30*, 1800295.
[68] R. Karthik, J. Vinoth Kumar, S.-M. Chen, C. Karuppiah, Y.-H. Cheng, V. Muthuraj, *ACS Appl. Mater. Interfaces* **2017**, *9*, 6547.
[69] H.-D. Wang, D. K. Sang, Z.-N. Guo, R. Cao, J.-L. Zhao, M. N. Ullah Shah, T.-J. Fan, D.-Y. Fan, H. Zhang, *Chin. Phys. B* **2018**, *27*, 087308.
[70] M. Qiu, D. Wang, W. Liang, L. Liu, Y. Zhang, X. Chen, D. K. Sang, C. Xing, Z. Li, B. Dong, F. Xing, D. Fan, S. Bao, H. Zhang, Y. Cao, *Proc. Natl. Acad. Sci. USA* **2018**, *115*, 501.
[71] M. Qiu, A. Singh, D. Wang, J. Qu, M. Swihart, H. Zhang, P. N. Prasad, *Nano Today* **2019**, *25*, 135.
[72] F. Yin, K. Hu, S. Chen, D. Wang, J. Zhang, M. Xie, D. Yang, M. Qiu, H. Zhang, Z.-g. Li, *J. Mater. Chem. B* **2017**, *5*, 5433.
[73] T. Fan, Y. Zhou, M. Qiu, H. Zhang, *J. Innovative Opt. Health Sci.* **2018**, *11*, 1830003.
[74] C. Xing, S. Chen, M. Qiu, X. Liang, Q. Liu, Q. Zou, Z. Li, Z. Xie, D. Wang, B. Dong, L. Liu, D. Fan, H. Zhang, *Adv. Healthcare Mater.* **2018**, *7*, 1701510.
[75] C. Xing, G. Jing, X. Liang, M. Qiu, Z. Li, R. Cao, X. Li, D. Fan, H. Zhang, *Nanoscale* **2017**, *9*, 8096.
[76] M. Qiu, W. X. Ren, T. Jeong, M. Won, G. Y. Park, D. K. Sang, L.-P. Liu, H. Zhang, J. S. Kim, *Chem. Soc. Rev.* **2018**, *47*, 5588.
[77] J. Jiang, J. Guo, X. Wan, Y. Yang, H. Xie, D. Niu, J. Yang, J. He, Y. Gao, Q. Wan, *Small* **2017**, *13*, 1700933.
[78] V. K. Sangwan, D. Jariwala, I. S. Kim, K.-S. Chen, T. J. Marks, L. J. Lauhon, M. C. Hersam, *Nat. Nanotechnol.* **2015**, *10*, 403.
[79] H. Tian, Q. Guo, Y. Xie, H. Zhao, C. Li, J. J. Cha, F. Xia, H. Wang, *Adv. Mater.* **2016**, *28*, 4991.
[80] L. Zhang, T. Gong, H. Wang, Z. Guo, H. Zhang, *Nanoscale* **2019**, *11*, 12413.
[81] A. Luican, G. Li, A. Reina, J. Kong, R. R. Nair, K. S. Novoselov, A. K. Geim, E. Y. Andrei, *Phys. Rev. Lett.* **2011**, *106*, 126802.
[82] J. M. B. L. dos Santos, N. M. R. Peres, A. H. Castro Neto, *Phys. Rev. Lett.* **2007**, *99*, 256802.
[83] Y. Cao, V. Fatemi, A. Demir, S. Fang, S. L. Tomarken, J. Y. Luo, J. D. Sanchez-Yamagishi, K. Watanabe, T. Taniguchi, E. Kaxiras, R. C. Ashoori, P. Jarillo-Herrero, *Nature* **2018**, *556*, 80.
[84] Y. Cao, V. Fatemi, S. Fang, K. Watanabe, T. Taniguchi, E. Kaxiras, P. Jarillo-Herrero, *Nature* **2018**, *556*, 43.
[85] R. Ribeiro-Palau, C. J. Zhang, K. Watanabe, T. Taniguchi, J. Hone, C. R. Dean, *Science* **2018**, *361*, 690.
[86] N. Lu, H. Guo, Z. Zhuo, L. Wang, X. Wu, X. C. Zeng, *Nanoscale* **2017**, *9*, 19131.
[87] M. Yankowitz, J. M. Xue, D. Cormode, J. D. Sanchez-Yamagishi, K. Watanabe, T. Taniguchi, P. Jarillo-Herrero, P. Jacquod, B. J. LeRoy, *Nat. Phys.* **2012**, *8*, 382.
[88] C. R. Dean, L. Wang, P. Maher, C. Forsythe, F. Ghahari, Y. Gao, J. Katoch, M. Ishigami, P. Moon, M. Koshino, T. Taniguchi, K. Watanabe, K. L. Shepard, J. Hone, P. Kim, *Nature* **2013**, *497*, 598.
[89] H. Yu, G.-B. Liu, J. J. Tang, X. D. Xu, W. Yao, *Sci. Adv.* **2017**, *3*, e1701696.
[90] K. Tran, G. Moody, F. C. Wu, X. B. Lu, J. Choi, K. Kim, A. Rai, D. A. Sanchez, J. M. Quan, A. Singh, J. Embley, A. Zepeda, M. Campbell, T. Autry, T. Taniguchi, K. Watanabe, N. S. Lu, S. K. Banerjee, K. L. Silverman, S. Kim, E. Tutuc, L. Yang, A. H. MacDonald, X. Q. Li, *Nature* **2019**, *567*, 71.
[91] K. L. Seyler, P. Rivera, H. Y. Yu, N. P. Wilson, E. L. Ray, D. G. Mandrus, J. Q. Yan, W. Yao, X. D. Xu, *Nature* **2019**, *567*, 66.
[92] S. Carr, S. Fang, P. Jarillo-Herrero, E. Kaxiras, *Phys. Rev. B* **2018**, *98*, 5.
[93] Y. Cao, J. Y. Luo, V. Fatemi, S. Fang, J. D. Sanchez-Yamagishi, K. Watanabe, T. Taniguchi, E. Kaxiras, P. Jarillo-Herrero, *Phys. Rev. Lett.* **2016**, *117*, 116804.
[94] K. Kim, A. DaSilva, S. Huang, B. Fallahazad, S. Larentis, T. Taniguchi, K. Watanabe, B. J. LeRoy, A. H. MacDonald, E. Tutuc, *Proc. Natl. Acad. Sci. USA* **2017**, *114*, 3364.

© 2020 WILEY-VCH Verlag GmbH & Co. KGaA, Weinheim

[95] F. Hu, S. R. Das, Y. Luan, T. F. Chung, Y. P. Chen, Z. Fei, *Phys. Rev. Lett.* **2017**, *119*, 247402.
[96] K. Kim, M. Yankowitz, B. Fallahazad, S. Kang, H. C. P. Movva, S. Huang, S. Larentis, C. M. Corbet, T. Taniguchi, K. Watanabe, S. K. Banerjee, B. J. LeRoy, E. Tutuc, *Nano Lett.* **2016**, *16*, 5968.
[97] S. Carr, D. Massatt, S. Fang, P. Cazeaux, M. Luskin, E. Kaxiras, *Phys. Rev. B* **2017**, *95*, 075420.
[98] J. M. Campanera, G. Savini, I. Suarez-Martinez, M. I. Heggie, *Phys. Rev. B* **2007**, *75*, 235449.
[99] d. L. r. G. Trambly, D. Mayou, L. Magaud, *Nano Lett.* **2010**, *10*, 804.
[100] A. Thomson, S. Chatterjee, S. Sachdev, M. S. Scheurer, *Phys. Rev. B* **2018**, *98*, 075109.
[101] J. Xue, J. Sanchez-Yamagishi, D. Bulmash, P. Jacquod, A. Deshpande, K. Watanabe, T. Taniguchi, P. Jarillo-Herrero, B. J. LeRoy, *Nat. Mater.* **2011**, *10*, 282.
[102] R. Decker, Y. Wang, V. W. Brar, W. Regan, H.-Z. Tsai, Q. Wu, W. Gannett, A. Zettl, M. F. Crommie, *Nano Lett.* **2011**, *11*, 2291.
[103] F. Varchon, P. Mallet, L. Magaud, J.-Y. Veuillen, *Phys. Rev. B* **2008**, *77*, 165415.
[104] D. L. Miller, K. D. Kubista, G. M. Rutter, M. Ruan, W. A. de Heer, P. N. First, J. A. Stroscio, *Phys. Rev. B* **2010**, *81*, 125427.
[105] F. Varchon, P. Mallet, J. Y. Veuillen, L. Magaud, *Phys. Rev. B* **2008**, *77*, 235412.
[106] C. Q. Shen, X. Z. Yan, F. Z. Qing, X. B. Niu, R. Stehle, S. S. Mao, W. L. Zhang, X. S. Li, *J. Materiomics* **2019**, *5*, 463.
[107] B. Deng, Z. F. Liu, H. L. Peng, *Adv. Mater.* **2019**, *31*, 25.
[108] H. Q. Ta, D. J. Perello, D. L. Duong, G. H. Han, S. Gorantla, V. L. Nguyen, A. Bachmatiuk, S. V. Rotkin, Y. H. Lee, M. H. Rummeli, *Nano Lett.* **2016**, *16*, 6403.
[109] C. Zhang, C.-P. Chuu, X. Ren, M.-Y. Li, L.-J. Li, C. Jin, M.-Y. Chou, C.-K. Shih, *Sci. Adv.* **2017**, *3*, e1601459.
[110] K. M. Omambac, H. Hattab, C. Brand, G. Jnawali, A. T. N'Diaye, J. Coraux, R. van Gastel, B. Poelsema, T. Michely, F. J. Meyer zu Heringdorf, *Nano Lett.* **2019**, *19*, 4594.
[111] B. Wang, M. Huang, N. Y. Kim, B. V. Cunning, Y. Huang, D. Qu, X. Chen, S. Jin, M. Biswal, X. Zhang, S. H. Lee, H. Lim, W. J. Yoo, Z. Lee, R. S. Ruoff, *Nano Lett.* **2017**, *17*, 1467.
[112] J. C. Rode, D. Zhai, C. Belke, S. J. Hong, H. Schmidt, N. Sandler, R. J. Haug, *2D Mater.* **2019**, *6*, 015021.
[113] X. D. Chen, W. Xin, W. S. Jiang, Z. B. Liu, Y. Chen, J. G. Tian, *Adv. Mater.* **2016**, *28*, 2563.
[114] K. M. Omambac, H. Hattab, C. Brand, G. Jnawali, A. T. N'Diaye, J. Coraux, R. van Gastel, B. Poelsema, T. Michely, F.-J. Meyer zu Heringdorf, M. H. -v. Hoegen, *Nano Lett.* **2019**, *19*, 4594.
[115] M. Yankowitz, S. Chen, H. Polshyn, Y. Zhang, K. Watanabe, T. Taniguchi, D. Graf, A. F. Young, C. R. Dean, *Science* **2019**, *363*, 1059.
[116] I. W. Frank, D. M. Tanenbaum, A. M. Van der Zande, P. L. McEuen, *J. Vac. Sci. Technol., B: Microelectron. Nanometer Struct.–Process., Meas., Phenom.* **2007**, *25*, 2558.
[117] C. Lee, X. Wei, J. W. Kysar, J. Hone, *Science* **2008**, *321*, 385.
[118] J. N. Grima, S. Winczewski, L. Mizzi, M. C. Grech, R. Cauchi, R. Gatt, D. Attard, K. W. Wojciechowski, J. Rybicki, *Adv. Mater.* **2015**, *27*, 1455.
[119] A. A. Balandin, S. Ghosh, W. Bao, I. Calizo, D. Teweldebrhan, F. Miao, C. N. Lau, *Nano Lett.* **2008**, *8*, 902.
[120] W. Cai, A. L. Moore, Y. Zhu, X. Li, S. Chen, R. S. Ruoff, *Nano Lett.* **2010**, *10*, 1645.
[121] A. A. Balandin, *Nat. Mater.* **2011**, *10*, 569.
[122] X. Xu, L. F. C. Pereira, Y. Wang, J. Wu, K. Zhang, X. Zhao, S. Bae, B. Cong Tinh, R. Xie, J. T. L. Thong, B. H. Hong, K. P. Loh, D. Donadio, B. Li, B. Oezyilmaz, *Nat. Commun.* **2014**, *5*, 3689.
[123] A. B. Kuzmenko, E. van Heumen, F. Carbone, D. van der Marel, *Phys. Rev. Lett.* **2008**, *100*, 4.
[124] F. Bonaccorso, Z. Sun, T. Hasan, A. C. Ferrari, *Nat. Photonics* **2010**, *4*, 611.
[125] K. F. Mak, L. Ju, F. Wang, T. F. Heinz, *Solid State Commun.* **2012**, *152*, 1341.
[126] D. N. Basov, M. M. Fogler, A. Lanzara, F. Wang, Y. B. Zhang, *Rev. Mod. Phys.* **2014**, *86*, 959.
[127] R. Saito, M. Fujita, G. Dresselhaus, M. S. Dresselhaus, *Phys. Rev. B* **1992**, *46*, 1804.
[128] R. Saito, M. Fujita, G. Dresselhaus, M. Dresselhaus, *Appl. Phys. Lett.* **1992**, *60*, 2204.
[129] T. Ohta, A. Bostwick, T. Seyller, K. Horn, E. J. S. Rotenberg, *Science* **2006**, *313*, 951.
[130] J. B. Oostinga, H. B. Heersche, X. Liu, A. F. Morpurgo, L. M. K. Vandersypen, *Nat. Mater.* **2008**, *7*, 151.
[131] S. D. Sarma, S. Adam, E. Hwang, E. Rossi, *Rev. Mod. Phys.* **2011**, *83*, 407.
[132] Y. Zhang, T.-T. Tang, C. Girit, Z. Hao, M. C. Martin, A. Zettl, M. F. Crommie, Y. R. Shen, F. Wang, *Nature* **2009**, *459*, 820.
[133] K. F. Mak, C. H. Lui, J. Shan, T. F. Heinz, *Phys. Rev. Lett.* **2009**, *102*, 256405.
[134] F. Xia, D. B. Farmer, Y. M. Lin, P. Avouris, *Nano Lett.* **2010**, *10*, 715.
[135] U. Soren, J. Jens Christian, C. Federico, J. A. Miwa, C. Alberto, Z. Michele, C. Cephise, C. Richard, S. Emma, M. Samir, *Phys. Rev. Lett.* **2014**, *112*, 257401.
[136] S. Lee, K. Lee, Z. Zhong, *Nano Lett.* **2010**, *10*, 4702.
[137] W. Liu, S. Kraemer, D. Sarkar, H. Li, P. M. Ajayan, K. Banerjee, *Chem. Mater.* **2014**, *26*, 907.
[138] W. Fang, A. L. Hsu, Y. Song, A. G. Birdwell, M. Amani, M. Dubey, M. S. Dresselhaus, T. Palacios, J. Kong, *ACS Nano* **2014**, *8*, 6491.
[139] V. L. Nguyen, D. J. Perello, S. Lee, C. T. Nai, B. G. Shin, J. G. Kim, H. Y. Park, H. Y. Jeong, J. Zhao, Q. A. Vu, *Adv. Mater.* **2016**, *28*, 8177.
[140] Y. Hao, L. Wang, Y. Liu, H. Chen, X. Wang, C. Tan, S. Nie, J. W. Suk, T. Jiang, T. Liang, *Nat. Nanotechnol.* **2016**, *11*, 426.
[141] X. Xu, C. Lin, F. Rui, S. Wang, H. Li, *AIP Adv.* **2016**, *6*, 820.
[142] F. Schwierz, *Nat. Nanotechnol.* **2010**, *5*, 487.
[143] A. Castellanos-Gomez, M. Buscema, R. Molenaar, V. Singh, L. Janssen, H. S. J. V. D. Zant, G. A. Steele, *2D Mater.* **2014**, *1*, 011002.
[144] L. Banszerus, M. Schmitz, S. Engels, J. Dauber, M. Oellers, F. Haupt, K. Watanabe, T. Taniguchi, B. Beschoten, C. Stampfer, *Sci. Adv.* **2015**, *1*, e1500222.
[145] W. S. Leong, H. Wang, J. Yeo, F. J. Martin-Martinez, A. Zubair, P.-C. Shen, Y. Mao, T. Palacios, M. J. Buehler, J.-Y. Hong, J. Kong, *Nat. Commun.* **2019**, *10*, 867.
[146] M. Sprinkle, D. Siegel, Y. Hu, J. Hicks, A. Tejeda, A. Taleb-Ibrahimi, P. Le Fèvre, F. Bertran, S. Vizzini, H. Enriquez, S. Chiang, P. Soukiassian, C. Berger, W. A. de Heer, A. Lanzara, E. H. Conrad, *Phys. Rev. Lett.* **2009**, *103*, 226803.
[147] S. Y. Zhou, G. H. Gweon, J. Graf, A. V. Fedorov, C. D. Spataru, R. D. Diehl, Y. Kopelevich, D. H. Lee, S. G. Louie, A. Lanzara, *Nat. Phys.* **2006**, *2*, 595.
[148] M. Sprinkle, D. Siegel, Y. Hu, J. Hicks, A. Tejeda, A. Taleb-Ibrahimi, P. Fèvre, Le, F. B , S. Vizzini, H. Enriquez, *Phys. Rev. Lett.* **2009**, *103*, 226803.
[149] B. Rafi, A. H. Macdonald, *Proc. Natl. Acad. Sci. USA* **2011**, *108*, 12233.
[150] J. Hass, R. Feng, T. Li, X. Li, Z. Zong, W. A. D. Heer, P. N. First, E. H. Conrad, C. A. Jeffrey, C. A. Berger, *Appl. Phys. Lett.* **2006**, *89*, 143106.
[151] I. Brihuega, P. Mallet, H. González-Herrero, G. Trambly de Laissardière, M. M. Ugeda, L. Magaud, J. M. Gómez-Rodríguez, F. Ynduráin, J. Y. Veuillen, *Phys. Rev. Lett.* **2012**, *109*, 196802.
[152] W. Yan, L. Meng, M. Liu, J.-B. Qiao, Z.-D. Chu, R.-F. Dou, Z. Liu, J.-C. Nie, D. G. Naugle, L. He, *Phys. Rev. B* **2014**, *90*, 115402.

© 2020 WILEY-VCH Verlag GmbH & Co. KGaA, Weinheim

[153] S.-Y. Li, K.-Q. Liu, L.-J. Yin, W.-X. Wang, W. Yan, X.-Q. Yang, J.-K. Yang, H. Liu, H. Jiang, L. He, *Phys. Rev. B* **2017**, *96*, 155416.
[154] A. Luican, G. Li, A. Reina, J. Kong, R. Nair, K. S. Novoselov, A. K. Geim, E. Andrei, *Phys. Rev. Lett.* **2011**, *106*, 126802.
[155] Z. Wang, F. Liu, M. Chou, *Nano Lett.* **2012**, *12*, 3833.
[156] E. S. Morell, J. Correa, P. Vargas, M. Pacheco, Z. Barticevic, *Phys. Rev. B* **2010**, *82*, 121407.
[157] P. Edwards, N. Mott, A. Alexandrov, *J. Supercond.* **1998**, *11*, 151.
[158] M. Imada, A. Fujimori, Y. Tokura, *Rev. Mod. Phys.* **1998**, *70*, 1039.
[159] E. A. Yelland, J. Singleton, C. H. Mielke, N. Harrison, F. F. Balakirev, B. Dabrowski, J. R. Cooper, *Phys. Rev. Lett.* **2008**, *100*, 047003.
[160] A. Bangura, J. Fletcher, A. Carrington, J. Levallois, M. Nardone, B. Vignolle, P. Heard, N. Doiron-Leyraud, D. LeBoeuf, L. Taillefer, *Phys. Rev. Lett.* **2008**, *100*, 047004.
[161] A. H. MacDonald, *Physics* **2019**, *12*, 12.
[162] Y. Jiang, X. Lai, K. Watanabe, T. Taniguchi, K. Haule, J. Mao, E. Y. Andrei, *Nature* **2019**, *573*, 91.
[163] A. Kerelsky, L. J. McGilly, D. M. Kennes, L. D. Xian, M. Yankowitz, S. W. Chen, K. Watanabe, T. Taniguchi, J. Hone, C. Dean, A. Rubio, A. N. Pasupathy, *Nature* **2019**, *572*, 95.
[164] Y. Xie, B. Lian, B. Jäck, X. Liu, C.-L. Chiu, K. Watanabe, T. Taniguchi, B. A. Bernevig, A. Yazdani, *Nature* **2019**, *572*, 101.
[165] Y. Cao, D. Rodan-Legrain, O. Rubies-Bigordà, J. M. Park, K. Watanabe, T. Taniguchi, P. Jarillo-Herrero, preprint arXiv: 1903.08596, **2019**, https://arxiv.org/pdf/1903.08596.pdf.
[166] M. S. Scheurer, *Nature* **2019**, *572*, 40.
[167] W. Yan, M. Liu, R.-F. Dou, L. Meng, L. Feng, Z.-D. Chu, Y. Zhang, Z. Liu, J.-C. Nie, L. He, *Phys. Rev. B* **2012**, *109*, 126801.
[168] K. Takeda, K. Shiraishi, *Phys. Rev. B* **1994**, *50*, 14916.
[169] P. Vogt, P. De Padova, C. Quaresima, J. Avila, E. Frantzeskakis, M. C. Asensio, A. Resta, B. Ealet, G. Le Lay, *Phys. Rev. Lett.* **2012**, *108*, 155501.
[170] L. Chen, C.-C. Liu, B. Feng, X. He, P. Cheng, Z. Ding, S. Meng, Y. Yao, K. Wu, *Phys. Rev. Lett.* **2012**, *109*, 056804.
[171] L. Tao, E. Cinquanta, D. Chiappe, C. Grazianetti, M. Fanciulli, M. Dubey, A. Molle, D. Akinwande, *Nat. Nanotechnol.* **2015**, *10*, 227.
[172] Y. Feng, D. Liu, B. Feng, X. Liu, L. Zhao, Z. Xie, Y. Liu, A. Liang, C. Hu, Y. Hu, *Proc. Natl. Acad. Sci. USA* **2016**, *113*, 14656.
[173] Y. Que, Y. Zhang, Y. Wang, L. Huang, W. Xu, J. Tao, L. Wu, Y. Zhu, K. Kim, M. Weinl, *Adv. Mater. Interfaces* **2015**, *2*, 1400543.
[174] Z. Li, J. Zhuang, L. Chen, Z. Ni, C. Liu, L. Wang, X. Xu, J. Wang, X. Pi, X. Wang, Y. Du, K. Wu, S. X. Dou, *ACS Cent. Sci.* **2016**, *2*, 517.
[175] F. Ya, F. Bao-Jie, X. Zhuo-Jin, L. Wen-Bin, L. Xu, L. De-Fa, Z. Lin, C. Lan, Z. Xing-Jiang, W. Ke-Hui, *Chin. Phys. Lett.* **2014**, *31*, 127303.
[176] R. Dombrowski, C. Steinebach, C. Wittneven, M. Morgenstern, R. Wiesendanger, *Phys. Rev. B* **1999**, *59*, 8043.
[177] Z. Li, J. Zhuang, L. Wang, H. Feng, Q. Gao, X. Xu, W. Hao, X. Wang, C. Zhang, K. Wu, *Sci. Adv.* **2018**, *4*, eaau4511.
[178] L. Li, Y. Yu, G. J. Ye, Q. Ge, X. Ou, H. Wu, D. Feng, X. H. Chen, Y. Zhang, *Nat. Nanotechnol.* **2014**, *9*, 372.
[179] A. Rodin, A. Carvalho, A. C. Neto, *Phys. Rev. Lett.* **2014**, *112*, 176801.
[180] H. Liu, A. T. Neal, Z. Zhu, Z. Luo, X. Xu, D. Tosmánek, P. D. Ye, *ACS Nano* **2014**, *8*, 4033.
[181] X. Zhou, R. Zhang, J. Sun, Y. Zou, D. Zhang, W. Lou, F. Cheng, G. Zhou, F. Zhai, K. Chang, *Sci. Rep.* **2015**, *5*, 12295.
[182] X. Zhou, W.-K. Lou, D. Zhang, F. Cheng, G. Zhou, K. Chang, *Phys. Rev. B* **2017**, *95*, 045408.
[183] F. Xia, H. Wang, Y. Jia, *Nat. Commun.* **2014**, *5*, 4458.
[184] R. Zhang, X. Zhou, D. Zhang, W. Lou, F. Zhai, K. Chang, *2D Mater.* **2015**, *2*, 045012.
[185] X. Zhou, W.-K. Lou, F. Zhai, K. Chang, *Phys. Rev. B* **2015**, *92*, 165405.
[186] D. Pan, T.-C. Wang, W. Xiao, D. Hu, Y. Yao, *Phys. Rev. B* **2017**, *96*, 041411.
[187] P. Kang, W. T. Zhang, V. Michaud-Rioux, X. H. Kong, C. Hu, G. H. Yu, H. Guo, *Phys. Rev. B* **2017**, *96*, 8.
[188] T. Fang, T. Liu, Z. Jiang, R. Yang, P. Servati, G. Xia, *ACS App. Nano Mater.* **2019**, *2*, 3138.
[189] T. Cao, Z. Li, D. Y. Qiu, S. G. Louie, *Nano Lett.* **2016**, *16*, 5542.
[190] S. Zhao, E. Wang, E. A. Üzer, S. Guo, K. Watanabe, T. Taniguchi, T. Nilges, Y. Zhang, B. Liu, X. Zou, preprint arXiv:03644, **2019**, https://arxiv.org/ftp/arxiv/papers/1912/1912.03644.pdf.
[191] J. Dai, X. C. Zeng, *J. Phys. Chem. Lett.* **2014**, *5*, 1289.
[192] S. Plimpton, *J. Comput. Phys.* **1995**, *117*, 1.
[193] V. Michaud-Rioux, L. Zhang, H. Guo, *J. Comput. Phys.* **2016**, *307*, 593.
[194] Y. Zhou, Y. Saad, M. L. Tiago, J. R. Chelikowsky, *Phys. Rev. E* **2006**, *74*, 066704.
[195] B. Hunt, J. Sanchez-Yamagishi, A. Young, M. Yankowitz, B. J. LeRoy, K. Watanabe, T. Taniguchi, P. Moon, M. Koshino, P. Jarillo-Herrero, *Science* **2013**, *340*, 1427.
[196] Z. Zhang, G. Ouyang, *ACS Appl. Energy Mater.* **2018**, *1*, 5675.
[197] M. Le Ster, T. Maerkl, P. J. Kowalczyk, S. A. Brown, *Phys. Rev. B* **2019**, *99*, 075422.
[198] G. Chen, L. Jiang, S. Wu, B. Lyu, H. Li, B. L. Chittari, K. Watanabe, T. Taniguchi, Z. Shi, J. Jung, Y. Zhang, F. Wang, *Nat. Phys.* **2019**, *15*, 237.
[199] K. F. Mak, C. Lee, J. Hone, J. Shan, T. F. Heinz, *Phys. Rev. Lett.* **2010**, *105*, 136805.
[200] B. Radisavljevic, A. Radenovic, J. Brivio, V. Giacometti, A. Kis, *Nat. Nanotechnol.* **2011**, *6*, 147.
[201] Q. H. Wang, K. Kalantar-Zadeh, A. Kis, J. N. Coleman, M. S. Strano, *Nat. Nanotechnol.* **2012**, *7*, 699.
[202] K. Roy, M. Padmanabhan, S. Goswami, T. P. Sai, G. Ramalingam, S. Raghavan, A. Ghosh, *Nat. Nanotechnol.* **2013**, *8*, 826.
[203] D. Xiao, G.-B. Liu, W. Feng, X. Xu, W. Yao, *Phys. Rev. Lett.* **2012**, *108*, 196802.
[204] W. Yao, D. Xiao, Q. Niu, *Phys. Rev. B* **2008**, *77*, 235406.
[205] A. Splendiani, L. Sun, Y. Zhang, T. Li, J. Kim, C.-Y. Chim, G. Galli, F. Wang, *Nano Lett.* **2010**, *10*, 1271.
[206] W. Zhao, R. M. Ribeiro, M. Toh, A. Carvalho, C. Kloc, A. Castro Neto, G. Eda, *Nano Lett.* **2013**, *13*, 5627.
[207] F. Wu, T. Lovorn, A. H. Macdonald, *Phys. Rev. B* **2018**, *97*, 035306.
[208] H. Yu, Y. Wang, Q. Tong, X. Xu, W. Yao, *Phys. Rev. Lett.* **2015**, *115*, 187002.
[209] H. Yu, G.-B. Liu, J. Tang, X. Xu, W. Yao, *Sci. Adv.* **2017**, *3*, e1701696.
[210] M. H. Naik, M. Jain, *Phys. Rev. Lett.* **2018**, *121*, 266401.
[211] d. Z. Van, A M., J. Kunstmann, A. Chernikov, D. A. Chenet, Y. You, X. Zhang, P. Y. Huang, T. C. Berkelbach, L. Wang, F. Zhang, *Nano Lett.* **2014**, *14*, 3869.
[212] P.-C. Yeh, W. Jin, N. Zaki, J. Kunstmann, D. Chenet, G. Arefe, J. T. Sadowski, J. I. Dadap, P. Sutter, J. Hone, *Nano Lett.* **2016**, *16*, 953.
[213] S. Huang, X. Ling, L. Liang, J. Kong, H. Terrones, V. Meunier, M. S. Dresselhaus, *Nano Lett.* **2014**, *14*, 5500.
[214] K. Liu, L. Zhang, T. Cao, C. Jin, D. Qiu, Q. Zhou, A. Zettl, P. Yang, S. G. Louie, F. Wang, *Nat. Commun.* **2014**, *5*, 4966.
[215] A. Castellanos-Gomez, H. S. van der Zant, G. A. Steele, Nano Res. **2014**, *7*, 572.
[216] A. Castellanos-Gomez, M. Buscema, R. Molenaar, V. Singh, L. Janssen, H. S. van der Zant, G. A. Steele, *2D Mater.* **2014**, *1*, 011002.
[217] C. R. Dean, A. F. Young, I. Meric, C. Lee, L. Wang, S. Sorgenfrei, K. Watanabe, T. Taniguchi, P. Kim, K. L. Shepard, *Nat. Nanotechnol.* **2010**, *5*, 722.
[218] X. D. Chen, W. Xin, W. S. Jiang, Z. B. Liu, Y. Chen, J. G. Tian, *Adv. Mater.* **2016**, *28*, 2563.

© 2020 WILEY-VCH Verlag GmbH & Co. KGaA, Weinheim

[219] C. D. Zhang, C. P. Chuu, X. B. Ren, M. Y. Li, L. J. Li, C. H. Jin, M. Y. Chou, C. K. Shih, *Sci. Adv.* **2017**, *3*, 7.
[220] J. Feldmann, G. Peter, E. Göbel, P. Dawson, K. Moore, C. Foxon, R. Elliott, *Phys. Rev. Lett.* **1987**, *59*, 2337.
[221] S. Schmitt-Rink, D. Chemla, D. Miller, *Adv. Phys.* **1989**, *38*, 89.
[222] K. F. Mak, J. Shan, *Nat. Photonics* **2016**, *10*, 216.
[223] C. Gong, H. Zhang, W. Wang, L. Colombo, R. M. Wallace, K. Cho, *Appl. Phys. Lett.* **2013**, *103*, 053513.
[224] M.-H. Chiu, C. Zhang, H.-W. Shiu, C.-P. Chuu, C.-H. Chen, C.-Y. S. Chang, C.-H. Chen, M.-Y. Chou, C.-K. Shih, L.-J. Li, *Nat. Commun.* **2015**, *6*, 7666.
[225] X. Hong, J. Kim, S.-F. Shi, Y. Zhang, C. Jin, Y. Sun, S. Tongay, J. Wu, Y. Zhang, F. Wang, *Nat. Nanotechnol.* **2014**, *9*, 682.
[226] F. Ceballos, M. Z. Bellus, H.-Y. Chiu, H. Zhao, *ACS Nano* **2014**, *8*, 12717.
[227] H. Heo, J. H. Sung, S. Cha, B.-G. Jang, J.-Y. Kim, G. Jin, D. Lee, J.-H. Ahn, M.-J. Lee, J. H. Shim, *Nat. Commun.* **2015**, *6*, 7372.
[228] X. Zhu, N. R. Monahan, Z. Gong, H. Zhu, K. W. Williams, C. A. Nelson, *J. Am. Chem. Soc.* **2015**, *137*, 8313.
[229] A. F. Rigosi, H. M. Hill, Y. Li, A. Chernikov, T. F. Heinz, *Nano Lett.* **2015**, *15*, 5033.
[230] P. Rivera, J. R. Schaibley, A. M. Jones, J. S. Ross, S. Wu, G. Aivazian, P. Klement, K. Seyler, G. Clark, N. J. Ghimire, *Nat. Commun.* **2015**, *6*, 6242.
[231] H. Chen, X. Wen, J. Zhang, T. Wu, Y. Gong, X. Zhang, J. Yuan, C. Yi, J. Lou, P. M. Ajayan, *Nat. Commun.* **2016**, *7*, 12512.
[232] E. M. Alexeev, D. A. Ruiz-Tijerina, M. Danovich, M. J. Hamer, D. J. Terry, P. K. Nayak, S. Ahn, S. Pak, J. Lee, J. I. Sohn, *Nature* **2019**, *567*, 81.
[233] C. Jin, E. C. Regan, A. Yan, M. I. B. Utama, D. Wang, S. Zhao, Y. Qin, S. Yang, Z. Zheng, S. Shi, *Nature* **2019**, *567*, 76.
[234] A. C. Neto, F. Guinea, N. M. Peres, K. S. Novoselov, A. K. J. R. o. m. p. Geim, *Rev. Mod. Phys.* **2009**, *81*, 109.
[235] B. Urbaszek, A. Srivastava, *Nature* **2019**, *567*, 39.
[236] H. Hong, C. Liu, T. Cao, C. Jin, S. Wang, F. Wang, K. J. A. M. I. Liu, *Adv. Mater. Interf.* **2017**, *4*, 1601054.
[237] N. Liu, J. Zhang, S. Zhou, J. J. J. o. M. C. C. Zhao, *J. Mater. Chem. C* **2020**, *8*, 6264.

© 2020 WILEY-VCH Verlag GmbH & Co. KGaA, Weinheim